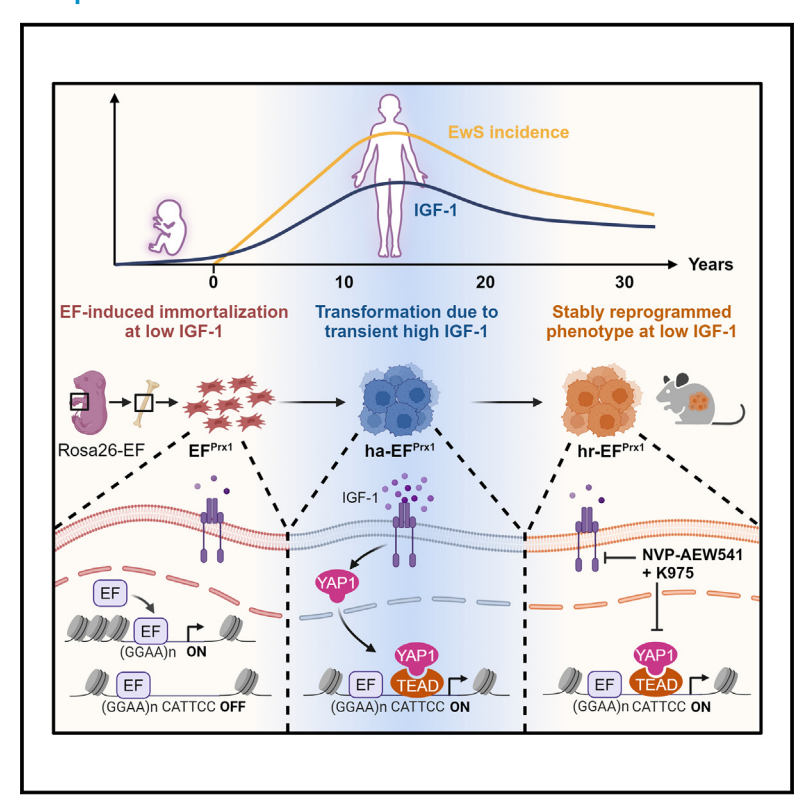
YAP1 is a key regulator of EWS::FLI1-dependent malignant transformation upon IGF-1-mediated reprogramming of bone mesenchymal stem cells

Graphical abstract



Authors

Rahil Noorizadeh, Barbara Sax, Tahereh Javaheri, ..., Florian Halbritter, Richard Moriggl, Heinrich Kovar

Correspondence

heinrich.kovar@ccri.at

In brief

Ewing sarcoma incidence follows IGF-1 serum levels during human development. Noorizadeh et al. report that low IGF-1 thresholds sustain viability of EWS::FLI1-mutant embryonal bone mesenchymal stem cell-like cells, but exposure to pubertal IGF-1 levels results in stable malignant transformation by a modular EWS::FLI1- and YAP1/TEAD-driven epigenetic mechanism.

Highlights

- Embryonal EWS::FLI1 expression in the bone mesenchyme causes skeletal abnormalities
- Exposure to pubertal IGF-1 levels transforms EWS::FLI1 mutant mouse mesenchymal stem cells
- EWS::FLI1 and IGF-1-induced Yap1 transform mesenchymal stem cells by a modular mechanism
- YAP1/TEAD and IGF-1R targeting compounds synergize to inhibit Ewing sarcoma cell growth







Article

YAP1 is a key regulator of EWS::FLI1-dependent malignant transformation upon IGF-1-mediated reprogramming of bone mesenchymal stem cells

Rahil Noorizadeh, ^{1,2} Barbara Sax, ³ Tahereh Javaheri, ³ Branka Radic-Sarikas, ^{1,4} Valerie Fock, ¹ Veveeyan Suresh, ¹ Maximilian Kauer, ¹ Aleksandr Bykov, ¹ Danijela Kurija, ⁵ Michaela Schlederer, ^{3,6} Lukas Kenner, ^{6,7,8,9,10} Gerhard Weber, ² Wolfgang Mikulits, ² Florian Halbritter, ¹ Richard Moriggl, ^{3,11,12} and Heinrich Kovar^{1,13,14,*}

SUMMARY

Ewing sarcoma (EwS) is an aggressive cancer of adolescents in need of effective treatment. Insulin-like growth factor (IGF)-1 is an autocrine growth factor for EwS, but only 10% of patients respond to IGF-1 receptor (IGF-1R) blockade. Although EwS is presumed to originate from mesenchymal progenitors during bone development, targeting of the EwS driver oncogene *EWS::FLI1* to the mesenchymal lineage in a mouse model does not result in tumor formation but in skeletal malformations and perinatal death. We report that transient exposure to IGF-1 concentrations mimicking serum levels during puberty reprograms limb-derived mesenchymal cells of *EWS::FLI1*-mutant mice to stable transformation and tumorigenicity. We identify a modular mechanism of IGF-1-driven tumor promotion in the early steps of EwS pathogenesis, in which Yap1 plays a central role. Pharmacologic Yap1/Tead inhibition reverses the transformed phenotype of EWS::FLI1-expressing cells. Our data provide a rationale for combined IGF-1R and YAP/TEAD inhibition in the treatment of EwS patients.

INTRODUCTION

Ewing sarcoma (EwS) is a highly aggressive bone and soft-tissue cancer with a peak incidence during puberty. 1,2 The 5-year disease-free survival rate of patients with localized EwS is about 70%–80%, while only 20%–30% of patients with metastases survive beyond 5 years despite intensive multimodal treatment. Therefore, there is an urgent unmet need for more efficient therapeutic approaches in this group of patients. However, progress in the identification and validation of novel treatment options is limited by a paucity of preclinical *in vivo* models faithfully recapitulating the human disease. 4,5

EwS is characterized by a chromosomal translocation rearranging the *EWSR1* gene on chromosome 22 with an ETS transcription factor family gene, most commonly *FLI1*.⁶ The re-

sulting gene fusion encodes the oncogenic transcription factor EWS::FLI1 (EF), targeting the aberrant expression and processing of a large number of genes involved in cellular proliferation and transformation.² Previous studies have shown that EF acts as a unique pioneer factor at GGAA repeat sites, mediating a transition from closed to open chromatin and establishing an active enhancer state leading to the aberrant activation of many EwS hallmark genes.⁷⁻⁹ Despite extensive knowledge of EF-driven gene regulatory mechanisms, the generation of a genetic mouse model for EwS remains challenging due to the toxicity of EF to most cell types and body tissues.⁴ Early studies in mouse fibroblasts revealed dependence of EF-driven transformation on the expression of the insulin-like growth factor-1 receptor (IGF-1R).¹⁰ In addition, autocrine production of IGF-1 was demonstrated to depend on EF expression in EwS.^{11,12} In



¹St. Anna Children's Cancer Research Institute (CCRI), 1090 Vienna, Austria

²Center for Cancer Research, Comprehensive Cancer Center, Medical University of Vienna, 1090 Vienna, Austria

³Ludwig Boltzmann Institute for Cancer Research, 1090 Vienna, Austria

⁴Department of Pediatric Surgery, Medical University of Vienna, 1090 Vienna, Austria

⁵Department of Neurophysiology, Center for Brain Research, Medical University of Vienna, 1090 Vienna, Austria

⁶Department of Pathology, Department for Experimental and Laboratory Animal Pathology, Medical University of Vienna, 1090 Vienna, Austria

⁷Comprehensive Cancer Center, Medical University of Vienna, 1090 Vienna, Austria

⁸Unit of Laboratory Animal Pathology, University of Veterinary Medicine Vienna, 1210 Vienna, Austria

⁹Christian Doppler Laboratory for Applied Metabolomics, Medical University of Vienna, 1090 Vienna, Austria

¹⁰Center for Biomarker Research in Medicine (CBmed), 8010 Graz, Austria

¹¹Department of Biosciences and Medical Biology, Paris Lodron University of Salzburg, 5020 Salzburg, Austria

¹²Institute of Animal Breeding and Genetics, University of Veterinary Medicine Vienna, 1210 Vienna, Austria

¹³Department of Pediatrics, Medical University of Vienna, 1090 Vienna, Austria

¹⁴Lead contact

^{*}Correspondence: heinrich.kovar@ccri.at https://doi.org/10.1016/j.celrep.2025.115381



fact, evidence suggests that EF creates a cellular environment conducive to IGF-1R signaling. EF directly activates the IGF-1 promoter¹¹ and simultaneously suppresses IGF-1R signalingmodulatory pathways through downregulation of several IGF-1- and IGF-1R-targeting microRNAs. 13 In addition, EF directly suppresses transcription as well as pappalysine-1-mediated degradation of negative regulatory IGF-1-binding proteins (IGFBPs). 14,15 Consequently, experimental silencing of EF expression resulted in impaired IGF-1R signaling. 16 Conversely, blocking IGF-1 signaling by IGF-1R antagonists, either antibodies or small-molecule inhibitors, inhibited EwS growth in athymic mice. 17 However, only 10%-14% of patients responded to IGF-1R-directed therapy in clinical trials, 18-20 at least in part due to upregulation of the closely related and interconnected insulin receptor signaling pathway, where both receptors form heterodimers.²¹ Collectively, these results demonstrate dependence of sustained EwS growth on EF-driven autocrine IGF-1/insulin signaling, but the status and role of this pathway at early stages of EwS pathogenesis remain unknown.

Identification of the embryonic stem cell of origin and its developmental stage is crucial to understand EwS initiation and progression. Neural crest- and mesoderm-derived mesenchymal stem cell (MSC) compartments are widely considered candidate progenitor cell types for EwS.^{22–25} Consistent with this hypothesis, targeting transgenic EF expression to the mesenchymal lineage in p53-knockout mice accelerated sarcoma formation,²⁶ but both germline and somatic p53 alterations are rare in human EwS, with an incidence below 10%.^{27–29}

We took a similar approach to restrict EF expression to the mesenchymal lineage during endochondral bone formation and confirmed that early expression of EF during embryogenesis is associated with severe skeletal malformations due to differentiation arrest at an early chondrocytic stage, leading to death of the progeny a few hours after birth. As EwS incidence in humans peaks during the second decade of life, a developmental period in which several growth-promoting hormones are highly enriched in the bone microenvironment, 30,31 we hypothesized that this endocrine milieu may play a tumor-promoting role in EwS pathogenesis. Interaction between tumor cells, tumorderived humoral factors, and the bone marrow in the bone niche has been shown to be essential for bone tumor initiation and progression. 32,33 We focused on IGF-1, which is known for its antiapoptotic activity through upregulation of Bcl2 family genes.³⁴ In the bone niche, IGF-1 is expressed from osteocytes and osteoblasts in response to mechanical load stimulating chondrocyte differentiation and bone growth. 35,36 Here, we provide evidence that mouse embryonal EF-expressing limb-derived MSC-like cells (MSCLCs) can be fully and stably transformed if transiently exposed to human pubertal serum IGF-1 levels, a condition that EwS precursor cells may experience in the bone niche during adolescence. We describe a modular reprogramming mechanism resulting in the activation of EwS hallmark genes with previously documented roles in EwS growth and survival and identify a key functional role for the transcriptional co-regulator Yap1 and its Tead transcription factor effectors. Our study provides a mechanism underlying the trajectories from EF-driven immortalization to full transformation caused by the activation of bone developmental signaling cues.

RESULTS

Embryonal expression of EF in the mesenchymal lineage impairs endochondral bone formation

We restricted EF expression to the mesenchymal lineage of endochondral bone formation by crossing a mouse line carrying a loxP-STOP-loxP-hemagglutinin (HA)-tagged EF cassette knocked into the Rosa26 locus37 to a Prx1-Cre transgenic line.³⁸ Mesenchymal targeting of Cre recombinase led to deletion of the STOP cassette, allowing for Rosa26 promoter-driven expression of HA-tagged EF in the developmental limb mesenchyme, starting from embryonal day (E) 9.538 (Figures S1A and S1E-S1G). The resulting mice (hereafter referred to as EFPrx1) displayed severe skeletal malformations, including polydactyly, short limbs, craniofacial malformations, and lack of rib cage closure (Figures S1B and S1C). They demonstrated absence of calcification in EFPrx1 limbs, sternum, and head bone calvaria (Figure S1C) and presence of only condensed cartilaginous elements with a lack of a hypertrophic zone and only patchy expression of chondrocytes (Ihh and Col10a1) and loss of osteoblast markers (Runx2, Osx, and Osc) (Figure S1D). All mice died within \sim 12 h of birth. Together, these results indicate an EF-induced developmental differentiation arrest of MSCLCs at an early chondrocytic stage during endochondral bone formation.

Characterization of limb-derived MSCLCs from EF mutant mice

To more closely characterize the molecular underpinnings of the observed differentiation arrest, we isolated and propagated MSCLCs from the limbs of two newborn EF^{Prx1} (#1 and #2) and wild-type (WT) Prx1-Cre mice. EF^{Prx1} MSCLCs stably expressed EF protein (Figure S2A) and were morphologically (Figure S2B) and immunophenotypically similar to WT MSCLCs, staining positive for mesenchymal markers CD90.2 and CD44 and negative for hematopoietic lineage markers CD45 and CD19 (Figure S2C). However, when incubated with the appropriate cytokine cocktails, EF^{Prx1} MSCLCs retained chondrocytic differentiation potential but failed to differentiate into adipocytic and osteoblastic lineages, while WT controls were able to differentiate into all three lineages (Figure S2D).

RNA sequencing (RNA-seq) analysis identified several antiapoptotic Bcl2a family members among 2,669 genes significantly downregulated in EF^{Prx1} MSCLCs compared to WT MSCLCs (DESeq2; $p_{adj} \leq 0.05$, $|log_2FC| \geq log_2(2))^{39}$ (Figures S3A and S3B; Tables S1 and S2). Among 1,610 genes that were found to be upregulated in EF^{Prx1} MSCLCs in comparison to WT MSCLCs, a significant enrichment of previously published human EF signature gene sets was observed (hypergeometric tests with hypeR; KINSEY_TARGETS_OF_EWSR1_FLII_FUSION_UP $p_{adj} = 0.00032$, RIGGI_EWING_SARCOMA_PROGENITOR_UP $p_{adj} = 0.068$; Figures S3C and S3D; Table S3).

In EwS, EF is known to gain the unique neomorphic ability to bind and open microsatellite sequences consisting of multiple "GGAA" repeats, turning them into transcriptional enhancers. ^{7,40,41} To monitor the effects of EF expression on global chromatin accessibility in our model, we applied the assay for transposase-accessible chromatin using sequencing (ATAC-seq) in EF^{Prx1} #1 and #2 versus WT MSCLCs (Tables S1



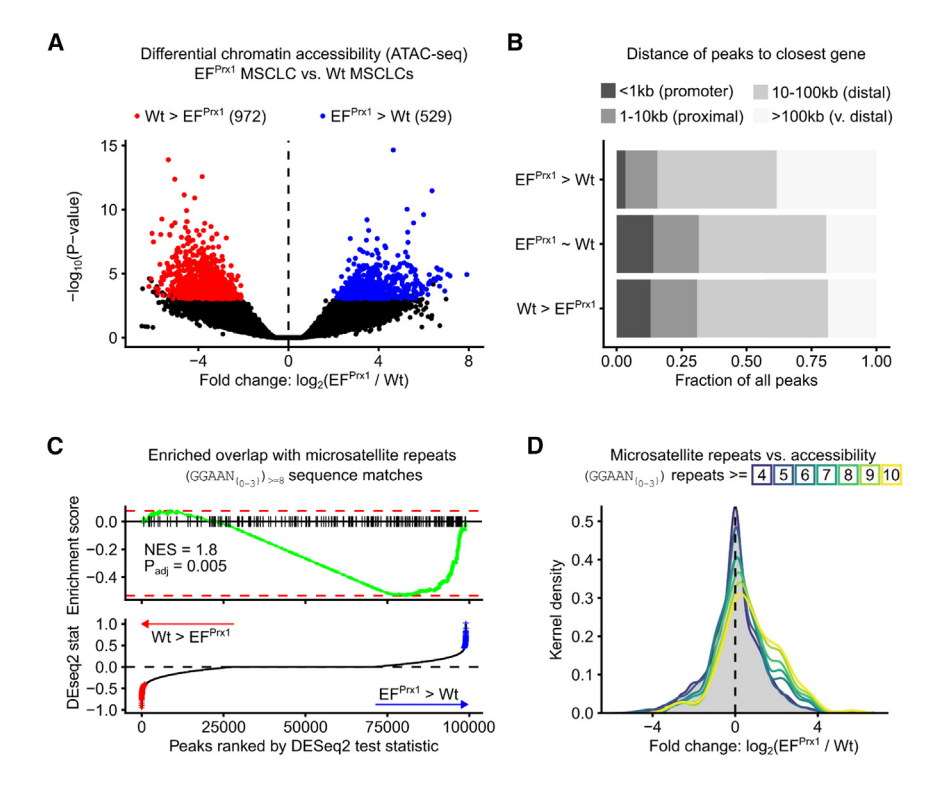


Figure 1. Chromatin accessibility is altered in EF^{Prx1} MSCLCs

(A) Volcano plot of differentially accessible chromatin regions between EF^{Prx1} MSCLCs and WT MSCLCs identified by DEseq2. The x axis indicates the logarithms of the fold changes of individual genes. The y axis indicates the negative logarithm of their p value to base 10 (DESeq2³⁹; $p_{\rm adj} < 0.05$, $|\log_2 {\rm FC}| > \log_2 (1.5)$; n [EF^{Prx1}] = 4, n [WT] = 3). See Tables S4 and S5.

(B) Distribution of differentially accessible peaks (from A) with respect to the distance from the transcription start site of the nearest gene compared to all regions without significant change (EF Prx1 MSCLCs \approx WT MSCLCs).

(C) Fast gene set enrichment analysis (fGSEA)⁴³ of GGAA microsatellite repeats in peaks that are more accessible in EF^{Prx1} MSCLCs than in WT MSCLCs. The barcode indicates peaks with at least eight repeats of the GGAA motif with a variable spacer of 0–3 bp. Peaks were preranked by the DESeq2 test statistic for the comparison of EF^{Prx1} MSCLCs and WT MSCLCs.

(D) Distribution of log₂ fold changes (between EF^{Prx1} MSCLCs and WT MSCLCs) in peaks separated by the number of repeats of the GGAA microsatellite within these peaks. The plot indicates the kernel density estimate per fold change value, which is similar to a histogram for continuous values.

and S4). We found 529 regions to have opened and 972 regions to have closed in EFPrx1 MSCLCs compared to the WT MSCLCs (Figure 1A and Table S5). The majority (84.3%) of ATAC-seq peaks gained in EF^{Prx1} MSCLCs were concentrated at a distance of more than 10 kb from the transcription start site (TSS) of the nearest gene, while 31.6% of peaks unaltered or lost in EFPrx1 MSCLCs in comparison to WT MSCLCs localized in proximal regions (<10 kb from the TSS) (Figure 1B). In addition, we found an enrichment of GGAA microsatellites in differentially opened regions of EFPrx1 MSCLCs (fast gene set enrichment analysis [fGSEA]; false discovery rate [FDR] = 0.005)43 (Figures 1C and 1D). Together, these data suggest that in mouse EFPrx1 MSCLCs, EF retains its neomorphic activity epigenetically reprogramming GGAA microsatellite enhancers.40 However, we cannot exclude that some of the chromatin accessibility differences between EFPrx1 MSCLCs and WT MSCLCs occurred as a consequence of oncogene-induced differentiation arrest at an early developmental chondrogenic stage and not due to a direct biochemical consequence of EF binding.

IGF-1 exposure assists EF in the stable transformation of limb-derived MSCLCs

Although EF^{Prx1} MSCLCs are immortal, they were unable to form colonies when plated at high dilution into soft agar (Figures 2A and 2B). Consistent with this *in vitro* finding, tumor formation was rarely observed, and if so, only with long latency, upon transplantation of EF^{Prx1} MSCLCs under the skin of SCID (C.B-17/IcrHsd-Prkcdscid) mice (Figure 2C). As the peak incidence of human EwS occurs during adolescence, in which several growth-promoting hormones, including IGF-1, are highly enriched in the bone microenvironment,³¹ we hypothesized that

embryonal limb-derived EFPrx1 MSCLCs may require additional stimuli from the endocrine milieu of the pubertal bone niche for full tumorigenic transformation. We focused on IGF-1 for its proposed essential role in sarcomagenesis.44 Since there is functional crosstalk between IGF-1R and insulin signaling in EwS,21 we also considered a potential role for insulin in the transformation process of mouse MSCLCs. To test our hypothesis, we plated EF^{Prx1} MSCLCs at a density of 1,000 cells/3.5 cm² dish in soft agar containing 10% fetal calf serum (FCS) in presence or absence of supplemented human IGF-1, insulin, or a combination of both at concentrations of 500 and 100 ng/mL, respectively, reflecting their peak serum levels during human puberty. 45,46 Hormone supplementation was renewed twice a week. After 4 weeks of incubation, anchorage-independent colonies became clearly visible in hormone-treated but rarely in control-treated plates of EFPrx1 MSCLCs (Figure 2A). The numbers of soft-agar colonies obtained after hormone treatment were similar for EF^{Prx1} MSCLCs from both mice (#1 and #2) and about 20-60 times higher than in untreated cultures and did not significantly differ between IGF-1, insulin, and combination treatments. No colonies were obtained for identically treated WT MSCLCs (data not shown). Since anchorage-independent growth in soft agar is commonly considered a surrogate for malignant transformation, these results suggested that hormone treatment had activated an EF-initiated transformation program. We, therefore, refer to cells from these colonies as "hormone-activated" (ha-) EFPrx1 MSCLCs (Figure 2A). ha-EF^{Prx1} MSCLCs showed only a marginally increased viability compared to parental EFPrx1 MSCLCs (Figure S4).

To test if the transformed phenotype required continuous hormone supplementation, we picked ha- ${\sf EF}^{\sf Prx1}$ MSCLC colonies



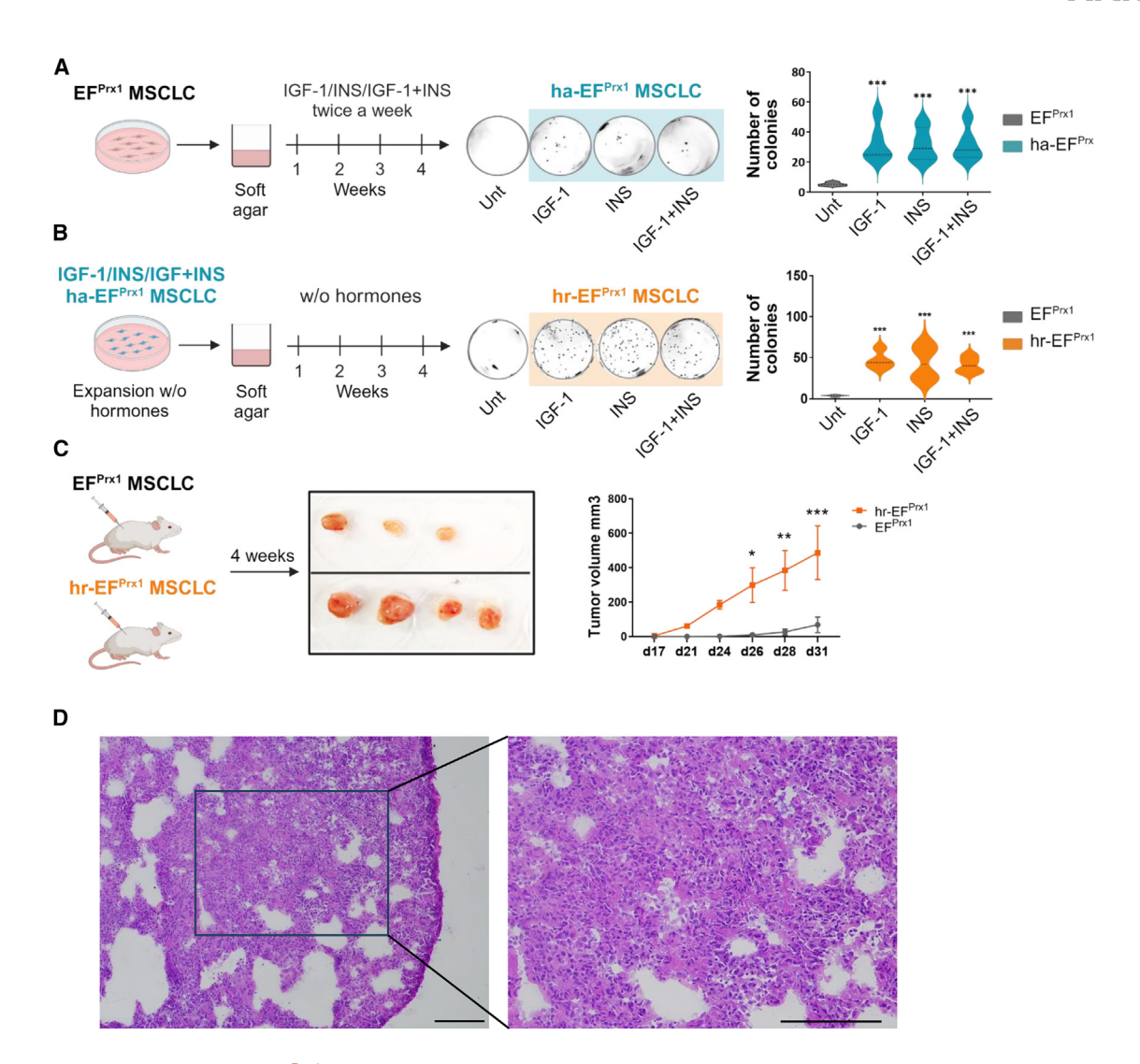


Figure 2. IGF-1 reprogramming of EF^{Prx1} MSCLC to full malignant transformation

(A) Approach assessing *in vitro* anchorage-independent growth of limb-derived MSCLCs from EF mutant mice as a surrogate of malignant transformation. EF^{Prx1} MSCLCs were grown in soft agar in the absence or presence of IGF-1 (500 ng/mL) and insulin (INS; 100 ng/mL) either alone or in combination according to the indicated scheme. Representative examples of soft-agar plates illustrating the appearance of transformed colonies after 4 weeks of incubation are shown. Cells derived from these colonies are referred to as hormone-activated (ha-) EF^{Prx1} MSCLCs. Colonies >0.5 mm were counted using ImageJ software. Results are presented as the mean ± SD of triplicate samples (hr-EF^{Prx1} MSCLC #2) from representative data of three independent experiments. Statistical significance was determined using one-way ANOVA (***rp < 0.0005). Unt, untreated (absence of IGF-1/INS).

(B) Same as in (A) but using ha-EF^{Prx1} cells as the starting material and culturing cells exclusively in the absence of hormone supplementation. Cells from colonies arising under these conditions are referred to as hormone-reprogrammed (hr-) EF^{Prx1} MSCLCs. Violin plots as in (A). n = 3. Statistical significance was determined using one-way ANOVA (***p < 0.0005).

(C) Tumor formation upon subcutaneous injection of parental EF^{Prx1} #2 and derived hr- EF^{Prx1} MSCLCs in SCID mice (n = 4 mice per group). The scheme, representative pictures, and mean tumor size increase over 31 days are shown. *p < 0.1, **p < 0.01, and ***p < 0.001.

(D) Hematoxylin and eosin stain of a frozen section of a representative tumor arising from the subcutaneous injection of hr-EF^{Prx1} MSCLCs in SCID mice. Scale bar: 100 μ m.

and expanded them in 10% FCS-containing growth medium for 5 days in the absence of IGF-1 and insulin supplementation before replating them in hormone-free soft agar for another 4 weeks. Strikingly, ha-EF^{Prx1} cells retained and even slightly increased their ability for anchorage-independent growth under hormone-free conditions, while this was not the case for control-treated cells (Figure 2B). We, therefore, refer to stably transformed cells isolated from colonies grown from ha-EF^{Prx1}

MSCLCs in the absence of further hormone treatment as "hormone-reprogrammed" (hr-) EF^{Prx1} MSCLCs. Notably, the transformed phenotype of hr-EF^{Prx1} MSCLCs remained dependent on continuous EF expression, as knockdown of the fusion protein drastically reduced their ability to grow in soft agar (Figure S5A). Intriguingly, hr-EF^{Prx1} MSCLCs gave rise to aggressively growing tumors with EwS-like small round cell morphology upon xenotransplantation into 8- to 10-week-old SCID mice, providing

Article



evidence for a complete and irreversibly transformed phenotype (Figures 2C and 2D). In contrast, transplantation of untreated parental EF^{Prx1} MSCLCs resulted in fewer and smaller tumors, which arose with much longer latency (Figure 2C).

WT MSCLCs, parental non-transformed EFPrx1 cells, and their transformed ha and hr derivatives were routinely propagated in 10% FCS-containing growth medium. FCS comprises multiple hormonal components at low concentrations, with IGF-1 amounts varying around 72 ng/mL. 47 Thus, the final concentration of IGF-1 in the basal growth medium containing 10% FCS is estimated to be about 70 times lower than the concentration (500 ng/mL) used for transformative reprogramming of EFPrx1 MSCLCs. We, therefore, tested the functional status of the IGF-1 signaling pathway in hr-EF^{Prx1} cells. When expanded in 10% FCS-containing growth medium, we observed tyrosine phosphorylation of the IGF-1R and serine phosphorylation of its downstream signaling effector AKT. which could be inhibited by the small-molecule IGF-1R-specific inhibitor NVP-AEW541.48 Under serum starvation, the signal was strongly reduced, consistent with paracrine IGF-1R activation, by the minute amounts of hormone contained in complete medium (Figure S5B). Human EwS cell lines are exquisitely sensitive to NVP-AEW541 at IC50 values around 200 nM.⁴⁹ In contrast, hr-EF^{Prx1} cells were largely resistant to the IGF-1R inhibitor treatment in adherent (IC50 = 9.3 μ M) and spheroid (IC50 = 3.7 μ M) growth conditions (Figure S5C). However, colony formation in soft agar was greatly reduced at NVP-AEW541 concentrations as low as 0.625 μ M (Figure S4D). Together, these results suggest that transient exposure to high concentrations of IGF-1 is needed for reprogramming EFPrx1 MSCLCs to full and stable malignant transformation, while low concentrations are still required for sustained clonogenic growth in soft agar.

IGF-1 reprogramming enforces an **EF** transcriptional signature

RNA-seq was performed for parental EFPrx1, ha-EFPrx1, and hr-EF^{Prx1} MSCLCs to analyze the transcriptomic changes associated with IGF-1 activation and reprogramming. Of 55,471 transcripts, 1,328 and 2,126 were found to be up- and downregulated (DESeq2; $p_{adi} \le 0.05$, $|log_2FC| \ge log_2(2)^{39}$) in ha-EF^{Prx1} versus parental cells, respectively (Table S6 and Figure 3A). Similarly, the expression of 1,079 and 1,732 genes was increased and decreased, respectively, in hr-EFPrx1 MSCLCs in comparison to untreated EFPrx1 MSCLCs (Table S7 and Figure 3A), roughly 42% (up) and 58% (down) of which overlapped with those in ha-EFPrx1 MSCLCs (Figure 3B). Strikingly, both shared up- and downregulated genes were significantly enriched in human EwS-derived EF target gene sets, including E2F and FOXM1 targets and genes associated with the epithelial-mesenchymal transition and extracellular matrix (ECM; Figures S6A and S6B and Table S8). However, the chromatin accessibility of only a few genomic regions was affected in hr-EF^{Prx1} MSCLCs compared to parental EF^{Prx1} MSCLCs (n =557) (Table S4), and there was no further enrichment in GGAA microsatellites in open chromatin regions, as tested by ATAC-seq (fGSEA; FDR = 0.083)⁴³ (Figures 3C and 3D). This result suggested that IGF-1 reprogramming did not significantly affect the neomorphic activity of EF on GGAA repeat regions but relied on different transcription regulatory mechanisms.

IGF-1 treatment-related chromatin accessibility changes identify modular mechanisms of EF^{Prx1} MSCLC reprogramming

To understand the transforming mechanisms by which transient IGF-1 exposure permanently reprograms EF^{Prx1} MSCLCs, we performed a comparative cluster analysis of open chromatin regions in untreated and IGF-1-treated WT MSCLCs, parental and hr-EF^{Prx1} MSCLCs #1 and #2, and one tumor obtained after transplantation of hr-EF^{Prx1} #1 (transplant-hr-EF^{Prx1} MSCLCs). Differentially accessible chromatin regions were classified in five distinct clusters designated modules M1 to M5 (Figure 4A and Table S4).

Cluster M1 comprises genomic regions that are closed in both EF^{Prx1} MSCLCs and hr-EF^{Prx1} MSCLCs but open in WT MSCLCs irrespective of IGF-1 treatment. Overrepresented genes enriched in the vicinity of these regions are involved in inflammatory responses and responses to cytokine stimuli (Figure S7A and Table S9). Conversely, cluster M4 contains chromatin regions that are closed in WT MSCLCs but open in parental and hr-EF^{Prx1} MSCLCs. Top enriched genes in the vicinity of these regions annotate to negative regulation of catabolic processes. In contrast, modules M2 and M3 comprise genomic regions that are exclusively open (M2) or closed (M3) in hr-EFPrx1 MSCLCs as a consequence of previous IGF-1 exposure. While there was no preferential enrichment of biological functions for nearby genes of cluster M3, top overrepresented M2 genes annotate to steroid hormone signaling. Taking a closer look, we observed that Yap1 and Lama5 were the most significant accessible genes among others, including EwS hallmark genes Prkcb,51 Bcl11b, 52,53 and Sox223,54,55 (Figure S7B). This is consistent with our RNA-seq findings, where there was an enrichment of Hippo pathway genes and specifically a significant upregulation of Yap1 and Lama5 on the transcriptional level upon IGF-1 reprogramming, which was corroborated on the protein level by immunoblotting (Figures 4B and 4C). Immunofluorescence staining identified induced Yap1 in both the cytoplasm and the nucleus of hr-EF^{Prx1} MSCLCs (Figure 4C). Consistent with an essential role of Yap1 in EFPrx1 MSCLC transformation, knockout of Yap1 in hr-EFPrx1 MSCLCs resulted in almost complete loss of colony formation (Figure 4E). Finally, M5 comprises chromatin regions that are not accessible in WT MSCLCs, are open in EF^{Prx1} MSCLCs, but which had reversed to a closed state upon IGF-1 reprogramming. Top enriched nearby genes associated with this cluster annotated to protein glycosylation (Figure S7A).

To better understand the gene regulatory mechanisms behind the individual modules, we identified transcription factor DNA binding motifs (from the JASPAR 2022 database⁵⁰) that were enriched in the differentially accessible chromatin clusters (Figure 4D and Table S9). Peaks specifically lost upon EF expression independent of IGF-1 (M1) were enriched in CCAAT box binding factor motifs, while top enriched motifs in those lost upon IGF-1 reprogramming in EF^{Prx1} MSCLCs are for KLF15, ZNF610, and ZNF93 in M3 and for PBX2, ETV1, and MEIS2 in M5. The EF and IGF-1 reprogramming-specific module M2 was found enriched in binding motifs for the retinoid acid receptor-related orphan nuclear receptor family, of which we found RorC to be expressed in hr-EF^{Prx1} MSCLCs (Figures 4D and S7C). However,



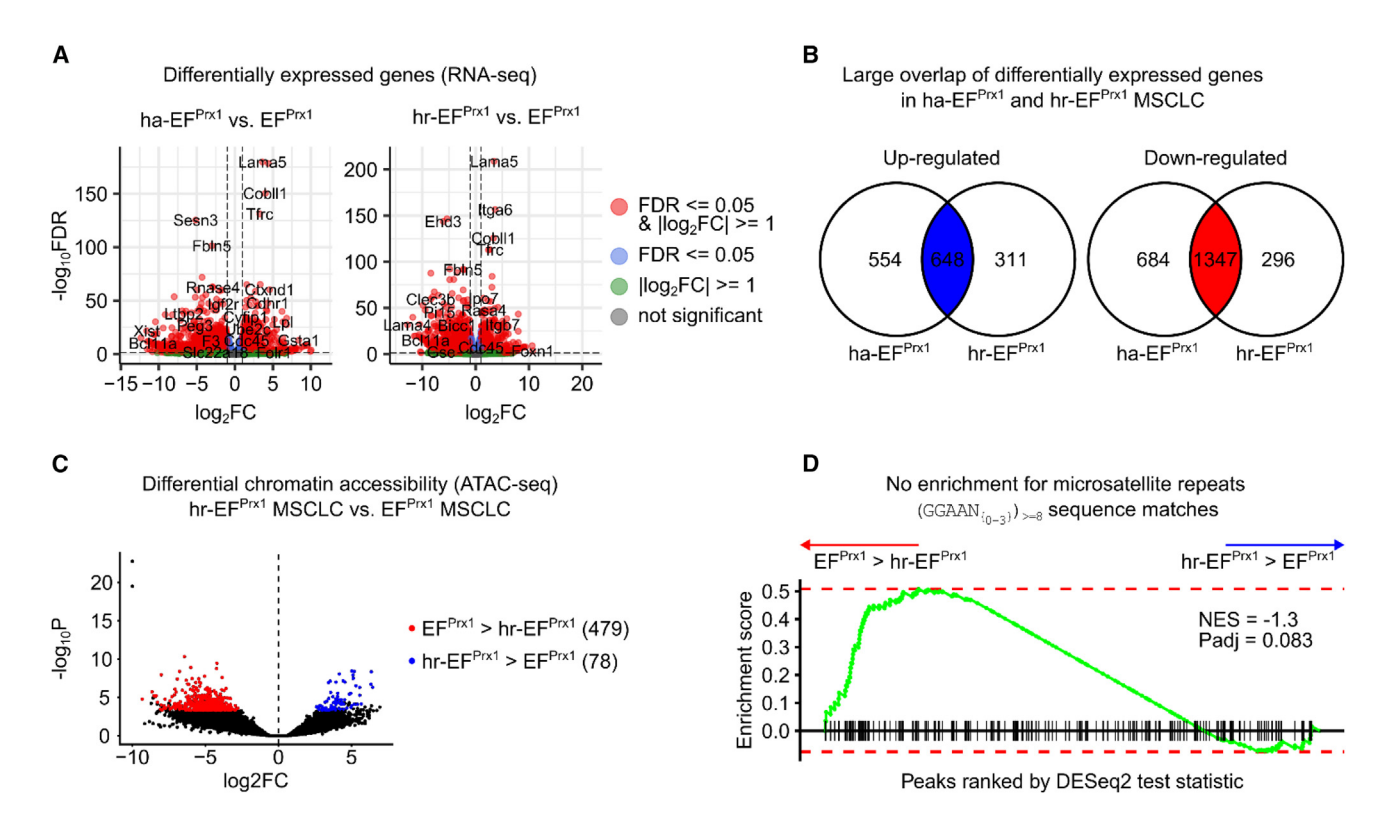


Figure 3. Transcriptional and chromatin changes associated with IGF-1 activation and reprogramming

(A) Volcano plot of differentially expressed genes between EF^{Prx1} MSCLCs and ha-EF^{Prx1} (left) or hr- EF^{Prx1} (right) MSCLCs identified by DEseq2. The x axis indicates the logarithm of the fold changes of individual genes. The y axis indicates the negative logarithm of their p value to base 10 (DESeq2³⁹; $p_{adj} < 0.05$, $|\log_2FC| > \log_2(2)$; n [EF^{Prx1}] = 2, n [ha-EF^{Prx1}] = 2, and n [hr-EF^{Prx1}] = 4). See Tables S6 and S7.

(B) Venn diagrams showing the overlap of differentially expressed genes between ha-EF^{Prx1} and hr-EF^{Prx1} MSCLCs for up- and downregulated genes in comparison to EF^{Prx1} MSCLCs (from A).

(C) Volcano plot of differentially accessible chromatin regions (from ATAC-seq) between hr-EF^{Prx1} MSCLCs and EF^{Prx1} MSCLCs. Each point represents an ATAC-seq peak, and significantly up- and downregulated regions are highlighted in blue and red, respectively (DESeq2³⁹; $p_{adj} < 0.05$, $|log_2FC| > log_2(1.5)$; n [hr-EF^{Prx1}] = 2 and n [EF^{Prx1}] = 4). See Table S5.

(D) Fast gene set enrichment analysis (fGSEA⁴³) of GGAA microsatellite repeats in peaks that are more accessible in hr-EF^{Prx1} MSCLCs compared to EF^{Prx1} MSCLCs. The barcode indicates peaks with at least eight repeats of the GGAA sequences with a variable spacer of 0–3 bp. Peaks were preranked by the DESeq2 test statistic for the comparison of hr-EF^{Prx1} MSCLCs and EF^{Prx1} MSCLCs.

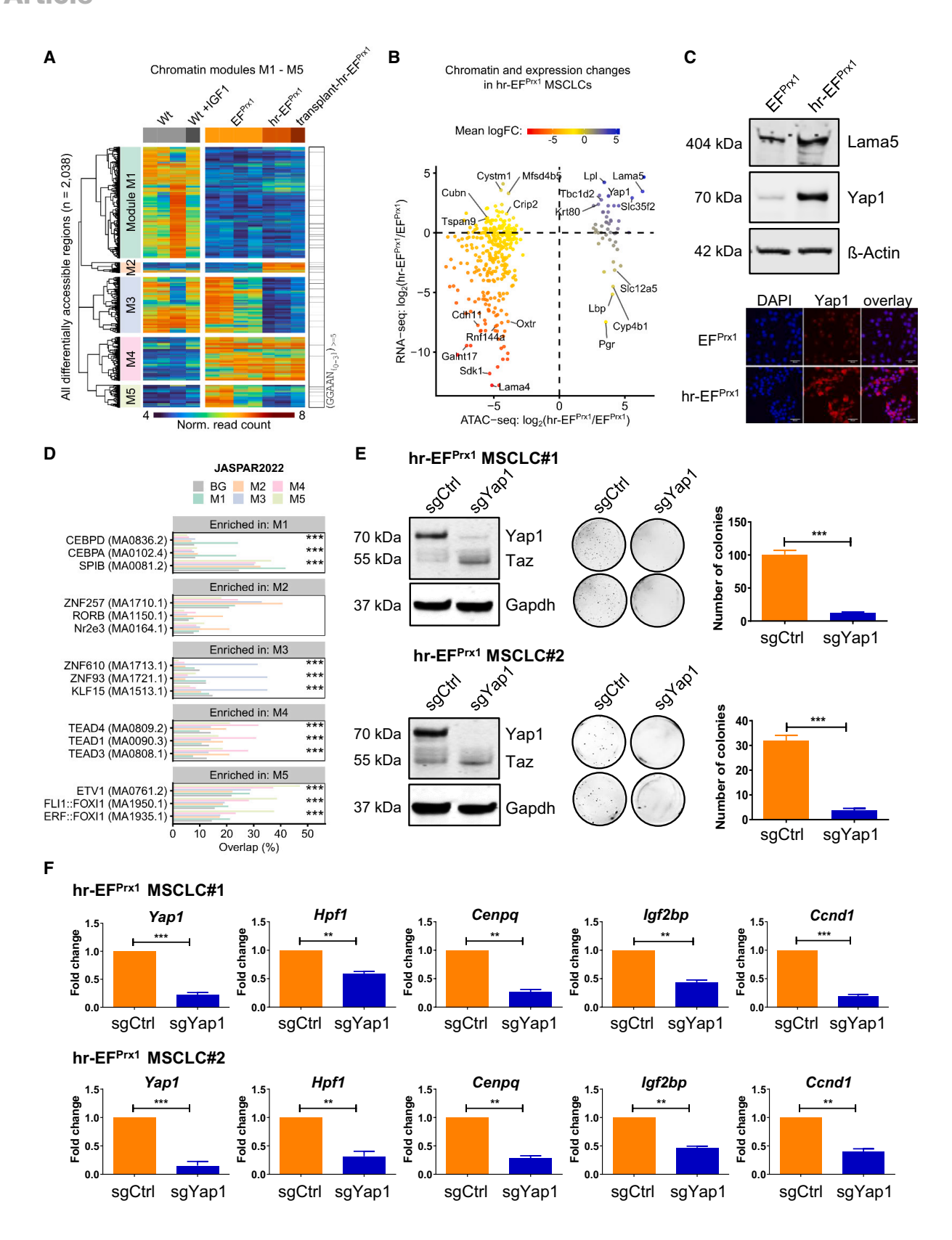
this enrichment was not statistically significant. Instead, we observed the highest incidence of GGAA microsatellites in M2. In contrast, and unexpectedly, the lowest frequency in GGAA repeats was present in M4 regions, which open up as a consequence of EF expression apparently unaffected by IGF-1 reprogramming (Figure 4A). Interestingly, the top and highly significantly enriched binding motif in M4 is that for Tead transcription factors, which are the downstream nuclear effectors of the Hippo signaling pathway (Figure 4D).

Sequential EF and IGF-1 signaling cooperate in the stepwise activation of TEAD target genes

As Tead transcription factor activity requires co-activation by Yap1, which we found to be induced as an M2 component exclusively upon IGF-1 reprogramming in EF-expressing MSCLCs, we wondered if a fraction of M4-associated genes may become activated in a stepwise manner by the sequential functional activity of the oncogenic fusion protein and IGF-1 signaling. Hence, we screened M4 genes for those that showed highly significant

TEAD binding motif accessibility in hr-EF^{Prx1} MSCLCs compared to EFPrx1 MSCLCs. Among them, we identified several genes with important functional roles in human EwS biology. We focused on Igf2bp1, a top EwS-specific dependency in DepMap⁵⁶; *Hpf1*, an essential co-factor of PARP1/2, which are highly expressed and therapeutic targets in EwS⁵⁷; Cenpq, a gene involved in the FoxM1/Plk-1/Cenp-A pathway of kinetochore assembly in mitotic progression^{58,59}; and the cell cycle regulator Ccnd1, which is overexpressed in EwS.60 Indeed, Yap1 knockout in hr-EF^{Prx1} MSCLCs resulted in downregulation of all these M4 genes, consistent with their expression being dependent on Yap1 activation in M2 (Figure 4F). In addition, Yap1 knockout also resulted in downregulation of FoxM1, identifying Yap1 as a major driver of the observed FoxM1 transcriptional signature imposed by IGF-1-mediated reprogramming of EF^{Prx1} MSCLCs (Figure S8). Together, these results suggest that malignant transformation of embryonal limb-derived MSCLCs in our EF mutant mouse model involved a modular mechanism, in which EF expression opened and primed





(legend on next page)



essential TEAD target genes for subsequent activation by IGF1-induced Yap1. In addition, we observed the emergence and variable expansion of *Yap1*-amplified subclones during propagation and IGF-1 reprogramming of bulk EF^{Prx1} MSCLCs, further strengthening the importance of sustained Yap1 expression to maintain the transformed phenotype (Figure S9A). However, minimal dilution and single-cell cloning experiments confirmed that Yap1 induction and phenotypic transformation of EF^{Prx1} MSCLCs by IGF-1 reprogramming occurred independent of *Yap1* copy number gains (Figures S9B–S9D).

To test if Yap1/Tead interaction was required to maintain the transformed phenotype of hr-EF^{Prx1} MSCLCs, we performed soft-agar colony assays in the absence and presence of the small-molecule TEAD-palmitoylation pocket binder K-975, which was previously shown to inhibit TEAD complex formation with its co-activator YAP1 in mesothelioma. Colony formation of hr-EF^{Prx1} MSCLCs was found to be drastically reduced already at nanomolar drug levels (Figure 5A), accompanied with downregulation of FoxM1 expression (Figure S8).

Since we had shown that colony formation of established hr-EF^{Prx1} cells remained sensitive to IGF-1R blockade, while anchorage-dependent growth was largely resistant to NVP-AEW541 treatment (Figures S5C and S5D), we tested if Yap/Tead inhibition might increase the sensitivity to IGF-1R blockade. Indeed, combination treatment with K-975 and NVP-AEW541 resulted in synergistic growth inhibition of hr-EF^{Prx1} cells (Figure 5B). Finally, we tested the drug combination in human EwS cell lines STA-ET-1 and SK-N-MC. The results confirmed that combined inhibition of IGF-1R and YAP1/TEAD is more effective against EwS than IGF-1R blockade alone (Figure 5C).

DISCUSSION

Based on the undifferentiated mesenchymal phenotype, EwS is considered an embryonal malignancy. However, clinical onset of the disease occurs mainly during the second decade of life. While available evidence clearly identifies expression of an EWS::ETS fusion protein as being causal for EwS pathogenesis, developmental timing of this pathognomonic rearrangement is unknown and may occur long before symptomatic disease. It

is possible that tumor initiation by the *EWSR1::ETS* gene rearrangement may long precede a tumorigenesis-promoting event. Although p53 mutation was identified as a genetic aberration greatly increasing EF-driven sarcomagenesis in mice and fish, ^{62,63} it is rare in EwS patients (<10%), and no other single recurrent genetic or epigenetic aberration has been associated with disease progression in humans so far.

Here, we tested the hypothesis that tumor initiation by a mutational mechanism happened during embryogenesis, leading to differentiation arrest and immortalization of a persisting mesenchymal osteochondrogenic precursor, while tumor promotion occurred by a non-genetic, humoral mechanism in the pubertal bone niche. Such a mechanism is difficult to model in vivo, as embryonal mesenchymal tissue expression of EF results in perinatal lethality. We therefore used explanted embryonal-limbderived MSCLCs from EF-mutant mice and subjected them to hormone treatment at a concentration that reflects serum levels during puberty, before assaying them for in vitro phenotypic signs of malignant transformation and in vivo tumorigenic potential upon transplantation into immune-compromised mice. This model allowed us to identify IGF-1/insulin signaling as a tumorpromoting mechanism for embryonal EF-expressing MSCLCs. Although EF^{Prx1} MSCLCs were routinely cultured in the presence of 10% FCS, the low IGF-1 concentrations contained in the growth medium did not suffice to promote cellular transformation. In contrast, transient (5 weeks) exposure to high IGF-1 concentrations stably transformed EFPrx1 MSCLCs to tumorigenicity. The choice of the transforming IGF-1 concentration (500 ng/mL) was oriented along peak serum levels, which are controlled by growth hormone during human puberty. 46 The actual levels of IGF-1 in the human bone niche, which is produced by various tissues during this developmental period, are not known. During the rapid pubertal growth spurt, which among primates is unique to humans, 64 mechanical load induces IGF-1 production from osteocytes and chondrocytes, 36 potentially further increasing its levels in the microenvironment of EF-induced EwS precursor cells. Again, this condition is difficult to model in mice, as IGF-1 knockout is perinatal lethal to 95% of offspring.⁶⁵ Even if the IGF-1 concentrations used in our experimental in vitro study may not fully reflect the actual in situ levels in the pubertal bone niche, they were sufficient to reproducibly

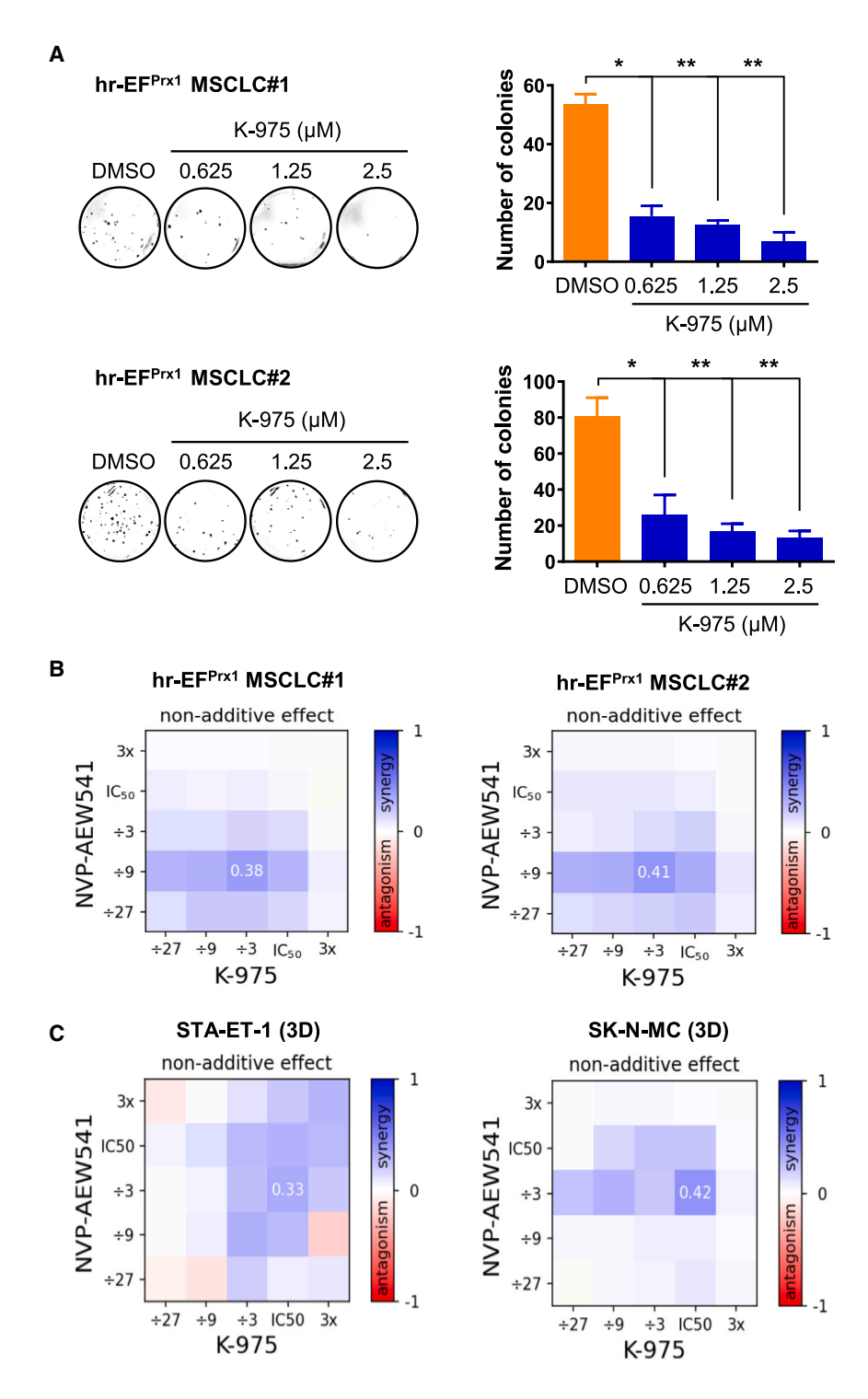
Figure 4. Comparative analysis of differentially accessible chromatin modules in MSCLCs

(A) Heatmap showing row-scaled normalized read counts for all peaks that were considered differentially accessible in at least one comparison (EF^{Prx1} MSCLCs/WT MSCLCs, hr-EF^{Prx1} MSCLCs/EF^{Prx1} MSCLCs, or MSCLC + IGF-1/WT MSCLCs; n_{total} = 2,038). Peaks are grouped into five "modules" (M1–M5). GGAA motif density in differentially open regions is indicated to the right of the heatmap. See Table S4.

- (B) Scatterplot comparing changes in the chromatin accessibility of ATAC-seq peaks (x axis) with the corresponding changes in gene expression of the nearest genes (y axis). One point is indicated for each combination of differentially accessible peak (from A) and differentially expressed gene. Color indicates the mean of both fold changes.
- (C) The protein levels of YAP1, LAMA5, and β -actin were detected by western blot for WT MSCLCs, EF^{Prx1} MSCLCs, and hr-EF^{Prx1} MSCLCs (top) and those of Yap1 by immunofluorescence staining (bottom). Scale bars: 50 μ m.
- (D) Bar plots showing DNA sequence motifs (mouse and human TF motifs from JASPAR 2022⁵⁰) overrepresented in peaks belonging to each of the five modules from (A). Each plot chart lists the top three motifs per module and each bar indicates the percentage of peaks with at least one match to the given motif. Enrichment was calculated using Fisher's exact test (one-tailed). * $^*p_{adj} < 0.05$, * $^*p_{adj} \le 0.01$, and * $^**^*p_{adj} \le 0.005$. See Table S9.
- (E) Left: Western blot analysis of YAP1 levels in hr-EF^{Prx1} MSCLCs #2 upon knockout of Yap1 using three CRISPR single-guide (sg)RNAs (sg-Yap1). Middle: Representative soft-agar assay for hr-EF^{Prx1} cells transduced with sg-Ctrl versus sg-Yap1. Right: The number of cell colonies was counted on days 21 after plating. Data are presented as the mean \pm SE (n = 3), ***p < 0.001. Statistics were calculated by one-tailed, paired Student's t test.
- (F) Quantitative analysis by RT-qPCR of relative mRNA expression levels of Yap1, Igf2bp1, Hpf1, Cenpq, and Ccnd1 after knockout of Yap1. Data are presented as the mean \pm SE (n = 3), ***p < 0.001 and **p < 0.001. Statistics were calculated by one-tailed, paired Student's t test.

Article





transform EF^{Prx1} MSCLCs from two independent founder mice, leading to rapid tumor formation upon xenotransplantation into 8- to 10-week-old SCID mice. In contrast, parental EFPrx1 MSCLCs generated much smaller tumors at lower frequency and longer latency. As IGF-1 serum levels in mice have been described to peak at around 900 ng/mL at 6 weeks of age and to gradually decline, with still 350 ng/mL at about 12 weeks of

Figure 5. YAP/TEAD blockade reduces colony-forming ability and synergizes with IGF-1R inhibition in hr-EFPrx1 MSCLCs and human EwS

(A) The effects of K-975 on soft-agar colony formation of hr-EFPrx1 MSCLCs upon 12 days incubation. Soft-agar assay shows a concentrationdependent decrease in the number of hr-EFPrx1 MSCLC colonies. Colonies >0.5 mm were counted using ImageJ software. Data are expressed as the mean \pm SD (n = 3); two-way ANOVA was used to determine statistical significance. **p < 0.01 and *p < 0.05.

(B) Overview of synergy scores of NVP-AEW541 and K-975 drug combinations across hr-EFPrx1 MSCLCs #1 and #2 in monolayer culture condi-

(C) Overview of synergy scores of NVP-AEW541 and K-975 drug combinations for STA-ET-1 and SK-N-MC human EwS cell lines in spheroid culture conditions. The heatmaps show Bliss excess across the hr-EFPrx1 MSCLCs (additive if =0 and non-additive if $\neq 0$; within non-additive cases, it is synergistic if >0 or antagonistic if <0).

age, 66 this observation may be explained by IGF-1 levels in transplanted mice being still high enough to promote in vivo tumorigenic reprogramming of EF^{Prx1} MSCLCs. Alternatively, we cannot exclude spontaneous transformation as the source of the tumors arising from the transplantation of parental EFPrx1 MSCLCs, as is frequently observed with cultured mouse bone marrow MSCs. 67,68

Before, it has been doubted that EwSlike tumorigenesis is possible in mice. mainly due to differences in GGAA microsatellite landscapes between mice and humans.4 Although on average, mice contain more and longer GGAA repeat regions than humans, their number and genomic locations relative to essential EwS genes vary significantly. Yet, it has been recently shown that transgenic EF alone can induce EwS-like tumors in the evolutionarily much more distant zebrafish.⁶⁹ In our mouse model, we find EFdriven GGAA microsatellite enrichment in open chromatin regions associated with a large number of genes partially overlapping with the human EwS signa-

ture. Among them, we find activation of the essential GGAA microsatellite-driven EwS hallmark genes Prkcb,51 the BAFcomplex component Bcl11b, 52,53 and the stemness factor Sox240,54,23 exclusively upon IGF-1-assisted transformation of EFPrx1 MSCLCs.

As another potential reason for previous failure to induce EwS tumorigenesis in mice, the well-documented toxicity of the EF



fusion protein to many cell types was discussed.⁴ Consistent with this supposition, we find downregulation of anti-apoptotic Bcl2 family members and increased apoptosis in EF^{Prx1} MSCLCs, which, however, did not interfere with their immortalization. Upon IGF-1 reprogramming, we observed decreased apoptosis and induction of anti-apoptotic Mcl-1, which is also found in human EwS, providing a potential therapeutic target.^{70,71}

While transcriptomic, epigenomic, and genomic analyses were sufficient to obtain mechanistic insights into the downstream transformation process leading to suppression of developmental programs (M3) and remodeling of stemness genes involved in self-renewal (M2 and M4; e.g., Sox2, Klf-5, Ccnd1, Bcl11b, etc.), the actual mechanism of stable transcriptional reprogramming by IGF-1/insulin remained largely elusive.

Canonical IGF-1 signaling involves activation of the PI3K/AKTmTOR and the RAS/MAPK-ERK pathways to induce cell growth and survival. 72 However, in addition to certain HDACs becoming phosphorylated by the PI3K/AKT axis leading to their exclusion from the nucleus, 73 more recent evidence identified a direct epigenetic role of nuclear-translocated IGF-1R directly binding to and remodeling chromatin via histone H3 phosphorylation and Brg1 recruitment. 74,75 Whether a similar mechanism might have been involved in the establishment of chromatin accessibility changes specifically found in clusters M2 and M3 of IGF-1 reprogrammed EF^{Prx1} MSCLCs remains to be established. In fact, only a small number of chromatin regions got opened in these cells in response to transient high IGF-1 exposure (M2). Here, binding motifs for retinoic acid receptor-like orphan receptors (RORA/B/C) were most prevalent. We found only RORC to be expressed in EF^{Prx1} MSCLCs independent of EF and IGF-1, making it unlikely that it was responsible for the observed IGF-1-induced chromatin accessibility changes. However, a recent chromatin immunoprecipitation sequencing (ChIP-seq) study revealed a strong overlap between RORA/C and glucocorticoid receptor (GR) chromatin binding at some 5,000 common enhancers and promoters of genes involved in lipid, fatty acid, and amino acid metabolism; the circadian clock; and PPARα activity in the mouse liver. 76 In line with this, functional annotation of M2 genes identified steroid hormone signaling and lipid metabolism as top enriched terms in this cluster. Intriguingly, EF acts as a transcriptional co-activator for GR in EwS.77 GR activation may have also contributed to the observed marked increase in Yap1 expression in EFPrx1 MSCLCs, similar to what was previously demonstrated for breast cancer in humans, where GR antagonists reduced YAP levels and inhibited cancer stem cell formation. 78,79 Consistent with our findings, there is evidence for an evolutionarily conserved PI3K-dependent but largely AKT-independent mechanism of Yki/Yap induction by IGF-1/insulin signaling, which feeds back on IGF-1/insulin signaling via direct upregulation of the insulin receptor.80 In addition, more recent studies in liver cancer and diffuse large B cell lymphoma revealed stabilization and activation of YAP1 nuclear translocation in response to IGF-1R signaling associated with poor prognosis.81,82

Insulin/IGF-1 signaling through PI3K is also required in the activation of Yki/Yap by mechanical and polarity cues. ⁸³ Mechanical tension is mediated via ECM components, specifically

laminin, communicating with integrins and cell adhesion molecules on the cell surface, leading through activation of focal adhesion and Src kinases to LATS1/2-dependent YAP1 activation. 79 We find the laminin 511 component LAMA5 to be highly induced by the combined activity of EF and IGF-1 in EF^{Prx1} MSCLCs impaired in osteogenic and adipogenic differentiation potential and unable to complete in vivo chondroblastic differentiation. Endogenously produced LAMA5 promotes self-renewal of human pluripotent stem cells (hPSCs) in an autocrine and paracrine manner through E-cadherin and FYN-RhoA-ROCK activation,84 and it is tempting to speculate that it fulfills a similar function in hr-EF^{Prx1} MSCLCs. Of note, the RhoA GAP Arhgap42 was also among highly upregulated hr-EF^{Prx1}-specific M2 genes in our study. In human MSCs, activation of the laminin receptor was shown to regulate OCT4 and SOX2 stem cell factor expression.⁸⁵ In our study, chromatin accessibility at the Sox2 locus was increased in hr-EFPrx1 cells together with activation of a further stem cell factor, KLF5 (Table S5), encoded in chromatin accessibility cluster M4 and known to be stabilized by Yap1 protein. 86 YAP1 appeared also involved in the observed upregulation of FOXM1 and its transcriptional program, as FoxM1 RNA and protein expression was greatly reduced upon Yap1/Tead inhibition by sgRNA or K-975. FOXM1 is a known mediator of EF-dependent cell-cycle regulation in EwS.87 Together, these results suggest that IGF-1 reprogramming of EFPrx1 MSCLCs enforces a stem cell program as the basis of malignant transformation.

The major finding of our study was that of a modular mechanism of stepwise malignant transformation by EF and IGF-1/insulin. In the first step, EF rewired the transcriptome of an embryonal osteochondrogenic precursor, resulting in developmental arrest and cellular immortalization. Here, the neomorphic activity of EF to bind and open GGAA microsatellites may have played an important role, which was, however, not sufficient to mediate full transformation. Instead, a large cluster of genes devoid of GGAA repeat regions but enriched in TEAD binding motifs (M4) opened in response to EF expression, priming them for binding and activation by the respective transcription factors. However, the actual activation of these genes occurred only upon induction of the co-activator Yap1 in the second reprogramming step following transient stimulation by high IGF-1/insulin. Although not required for IGF-1-driven full transformation, copy number gain at the Yap1 gene locus if present in a subclone of parental EF-expressing MSCLCs was positively selected in hr-EF^{Prx1} bulk cell populations. Yap1 amplification frequently occurs during human⁸⁸ and mouse⁸⁹⁻⁹⁵ tumorigenesis, though it has not yet been reported for EwS despite being highly expressed and associated with poor prognosis in this disease. 96

We hypothesize that Yap1 activation as a rate-limiting tumorigenic step occurs in the bone niche during puberty and further leads to epigenomic reprogramming resulting in suppression of heterogeneous developmental genes by an as yet unknown mechanism (M3 and M5) and the direct and indirect activation of a number of stemness and dependency genes involved in cell renewal, including Sox2, KLf5, and Igf2bp1, as well as key genes involved in cell cycle (i.e., Ccnd1), mitotic progression (i.e., FoxM1 and Cenpq), DNA repair (i.e., Hpf1), and survival (Mcl-1). Thus, it appears that the Hippo pathway played a key

Article



role in tumor initiation in our model. In contrast, in established human EwS tumors, this pathway has been associated with epithelial/mesenchymal-like transition and metastasis being activated upon EF modulation. In fact, in response to short hairpin RNA (shRNA)-mediated EF downregulation, we previously observed activation of TEAD target genes by the co-activators MRTFB and the YAP1 ortholog TAZ (WWTR1), while YAP1 was invariably expressed in all tested EwS cell lines, consistent with immunohistochemical positivity in a large fraction of primary EwS tumors. 96,97 Although the current scientific literature on Hippo pathway biology rarely distinguishes between YAP1 and TAZ, there is accumulating evidence that the two orthologous proteins may have different functions and regulate different TEAD target gene sets during normal limb development. 96,98,99 We therefore hypothesize that YAP1 may be essential for the onset of disease during puberty, while TAZ may drive metastasis of EwS. We therefore expect both activities to be sensitive to small-molecule inhibition of TEAD complex formation with its alternative co-activators YAP1 and TAZ, and accordingly, we have already shown that the metastatic potential of EwS is reduced by treatment with the YAP/TAZ/TEAD inhibitor verteporfin. 97 Here, we show that an allosteric TEAD inhibitor binding specifically to the TEAD palmitoylation pocket, K-975, greatly reduced the anchorage-independent colony-forming ability of hr-EF^{Prx1} MSCLCs and of EwS cell lines in vitro. Several related TEAD inhibitors have recently entered clinical trials for the treatment of high-risk solid tumors. 100 Our study provides a mechanistic rationale to combine YAP1/TEAD targeting compounds with IGF-1Rdirected therapy to improve the outcome of EwS patients. Here, we provide first proof-of-principle in vitro evidence for the efficacy of this combination in our model and in EwS cell lines, encouraging further preclinical development.

Limitations of the study

While our study provides an in vitro proof of concept for the potential role of high IGF-1 in the early steps of tumorigenic transformation of embryonal EF-expressing MSCLCs, a link to puberty was not formally tested in vivo. This would require a comparison of WT and tissue IGF-1-knockout mice as hosts in orthotopic transplantation models of EFPrx1 MSCLCs at different stages of adolescent mouse development. Furthermore, while our data revealed an important role for epigenetic Yap1 activation in the transformation process of EFPrx1 MSCLCs downstream of IGF-1 signaling, the exact mechanism by which transient IGF-1 exposure permanently activates Yap1 transcription remained elusive and requires further mechanistic studies. The important contribution of Yap1 in the transformation process is underlined by subclonal copy number gains, which were found to be positively selected during IGF-1 reprogramming. However, while this phenomenon has been reported in a number of cancers, 88-95 it has not yet been observed in EwS. Finally, our study provides a rationale for the combination of YAP1/TEAD and IGF-1R inhibitors for EwS. However, our lead drug (K975) was highly toxic in zebrafish xenografts, even at concentrations much lower than those showing synergy with IGF-1R inhibition in EwS cell lines in vitro (data not shown), and this drug was previously reported to cause renal toxicity in rodents, 101 thus making it clear that preclinical in vivo development of the proposed drug combination requires thorough dose determination studies in mice and less toxic, second-generation TEAD inhibitors.

RESOURCE AVAILABILITY

Lead contact

Requests for further information and resources and reagents should be directed to and will be fulfilled by the lead contact, Heinrich Kovar (heinrich. kovar@ccri.at).

Materials availability

EF^{Prx1} mice and xenografts of IGF-1-reprogrammed MSCLCs are available through ITCC-P4 gGmbH (https://www.itccp4.eu/) and the University of Veterinary Medicine, Vienna, Austria. EF^{Prx1} MSCLCs and hr-EF^{Prx1} MSCLCs are available at St. Anna Children's Cancer Research Institute GmbH, Vienna, Austria.

Data and code availability

- Data: the RNA-seq and ATAC-seq data generated in this study have been deposited at the Gene Expression Omnibus (GEO) and are publicly available as of the date of publication. Accession numbers are listed in the key resources table.
- Code: all original code has been deposited at GitHub and Zenodo and is publicly available as of the date of publication. Accession numbers are listed in the key resources table.
- Any additional information required to reanalyze the data reported in this
 paper is available from the lead contact upon request.

ACKNOWLEDGMENTS

We thank Drs. S. Baker and M. Logan for providing EF knockin and Prx1-Cre transgenic mice crossed to generate EF^{Prx1} mice. This research was funded in whole or in part by the European Union's Horizon 2020 Innovative Medicines Initiative H2020-IMI2-JTI-201 5-07, grant 116064 (ITCC P4); European Union's Horizon 2020 Research and Innovation Programme under the Marie Skłodowska-Curie grant agreement 956285 (VAGABOND); the Alex's Lemonade Stand Foundation (ALSF) "Crazy 8" grant 20-17258; and grants from the Austrian Science Fund (FWF) (P34341-B and P35353-B) to H.K.

AUTHOR CONTRIBUTIONS

Conceptualization, H.K. and R.M.; data curation, F.H. and M.K.; formal analysis, R.N., A.B., M.K., and F.H.; funding acquisition, H.K. and R.M.; investigation, R.N., B.S., B.R.-S., V.F., M.S., L.K., G.W., V.S., D.K., and T.J.; methodology, T.J., B.S., and B.R.-S.; project administration, H.K.; resources, T.J., W.M., L.K., and R.M.; software, F.H. and A.B.; supervision, H.K. and R.M.; visualization, R.N., F.H., A.B., and V.F.; writing – original draft, R.N. and H.K.; writing – review & editing, F.H., B.R.-S., V.F., and R.M.

DECLARATION OF INTERESTS

The authors declare no competing interests.

STAR***METHODS**

Detailed methods are provided in the online version of this paper and include the following:

- KEY RESOURCES TABLE
- EXPERIMENTAL MODEL AND STUDY PARTICIPANT DETAILS
 - o Genetically modified mice
 - Cell lines
- METHOD DETAILS
 - o Preparation and expansion of MSCLC
 - Skeletal staining
 - Histology
 - o RNA in situ hybridization





- o Flow cytometry
- Cell proliferation assay
- Differentiation assays
- Soft agar assay
- o In vivo tumor formation assay
- o SiRNA knockdown
- Viral Cas9 and sgRNA expression vectors
- Drug synergy assay
- RNA sequencing
- ATAC-seq
- Low coverage whole genome sequencing (lcWGS)
- QUANTIFICATION AND STATISTICAL ANALYSIS

SUPPLEMENTAL INFORMATION

Supplemental information can be found online at https://doi.org/10.1016/j.ceirep.2025.115381.

Received: August 14, 2024 Revised: December 15, 2024 Accepted: February 11, 2025

REFERENCES

- Davis, L., and Malempati, S. (2014). Ewing sarcoma in adolescents and young adults: diagnosis and treatment. Clin. Oncol. Adolesc. Young Adults 4, 21–31. https://doi.org/10.2147/COAYA.S61451.
- Grunewald, T.G.P., Cidre-Aranaz, F., Surdez, D., Tomazou, E.M., de Alava, E., Kovar, H., Sorensen, P.H., Delattre, O., and Dirksen, U. (2018). Ewing sarcoma. Nat. Rev. Dis. Primers 4, 5. https://doi.org/10. 1038/s41572-018-0003-x.
- Zollner, S.K., Amatruda, J.F., Bauer, S., Collaud, S., de Alava, E., DuBois, S.G., Hardes, J., Hartmann, W., Kovar, H., Metzler, M., et al. (2021). Ewing Sarcoma-Diagnosis, Treatment, Clinical Challenges and Future Perspectives. J. Clin. Med. 10, 1685. https://doi.org/10.3390/jcm10081685.
- Minas, T.Z., Surdez, D., Javaheri, T., Tanaka, M., Howarth, M., Kang, H.J., Han, J., Han, Z.Y., Sax, B., Kream, B.E., et al. (2017). Combined experience of six independent laboratories attempting to create an Ewing sarcoma mouse model. Oncotarget 8, 34141–34163. https://doi. org/10.18632/oncotarget.9388.
- Ramachandran, B., Rajkumar, T., and Gopisetty, G. (2021). Challenges in modeling EWS-FLI1-driven transgenic mouse model for Ewing sarcoma. Am. J. Transl. Res. 13, 12181–12194.
- Delattre, O., Zucman, J., Plougastel, B., Desmaze, C., Melot, T., Peter, M., Kovar, H., Joubert, I., de Jong, P., Rouleau, G., et al. (1992). Gene fusion with an ETS DNA-binding domain caused by chromosome translocation in human tumours. Nature 359, 162–165. https://doi.org/10. 1038/359162a0.
- Gangwal, K., Sankar, S., Hollenhorst, P.C., Kinsey, M., Haroldsen, S.C., Shah, A.A., Boucher, K.M., Watkins, W.S., Jorde, L.B., Graves, B.J., and Lessnick, S.L. (2008). Microsatellites as EWS/FLI response elements in Ewing's sarcoma. Proc. Natl. Acad. Sci. USA 105, 10149–10154.
- Riggi, N., Knoechel, B., Gillespie, S.M., Rheinbay, E., Boulay, G., Suvà, M.L., Rossetti, N.E., Boonseng, W.E., Oksuz, O., Cook, E.B., et al. (2014). EWS-FLI1 utilizes divergent chromatin remodeling mechanisms to directly activate or repress enhancer elements in Ewing sarcoma. Cancer. Cell. 26, 668–681. https://doi.org/10.1016/j.ccell.2014.10.004.
- Tomazou, E.M., Sheffield, N.C., Schmidl, C., Schuster, M., Schönegger, A., Datlinger, P., Kubicek, S., Bock, C., and Kovar, H. (2015). Epigenome mapping reveals distinct modes of gene regulation and widespread enhancer reprogramming by the oncogenic fusion protein EWS-FLI1. Cell Rep. 10, 1082–1095. https://doi.org/10.1016/j.celrep.2015.01.042.
- Toretsky, J.A., Kalebic, T., Blakesley, V., LeRoith, D., and Helman, L.J. (1997). The insulin-like growth factor-I receptor is required for EWS/

- FLI-1 transformation of fibroblasts. J. Biol. Chem. *272*, 30822–30827. https://doi.org/10.1074/jbc.272.49.30822.
- Cironi, L., Riggi, N., Provero, P., Wolf, N., Suvà, M.L., Suvà, D., Kindler, V., and Stamenkovic, I. (2008). IGF1 is a common target gene of Ewing's sarcoma fusion proteins in mesenchymal progenitor cells. PLoS One 3, e2634. https://doi.org/10.1371/journal.pone.0002634.
- Yee, D., Favoni, R.E., Lebovic, G.S., Lombana, F., Powell, D.R., Reynolds, C.P., and Rosen, N. (1990). Insulin-like growth factor I expression by tumors of neuroectodermal origin with the t(11;22) chromosomal translocation. A potential autocrine growth factor. J. Clin. Investig. 86, 1806–1814. https://doi.org/10.1172/JCI114910.
- McKinsey, E.L., Parrish, J.K., Irwin, A.E., Niemeyer, B.F., Kern, H.B., Birks, D.K., and Jedlicka, P. (2011). A novel oncogenic mechanism in Ewing sarcoma involving IGF pathway targeting by EWS/Fli1-regulated microRNAs. Oncogene 30, 4910–4920. https://doi.org/10.1038/onc. 2011.197.
- Prieur, A., Tirode, F., Cohen, P., and Delattre, O. (2004). EWS/FLI-1 silencing and gene profiling of Ewing cells reveal downstream oncogenic pathways and a crucial role for repression of insulin-like growth factor binding protein 3. Mol. Cell Biol. 24, 7275–7283. https://doi.org/10.1128/MCB.24.16.7275-7283.2004.
- Jayabal, P., Houghton, P.J., and Shiio, Y. (2017). EWS-FLI-1 creates a cell surface microenvironment conducive to IGF signaling by inducing pappalysin-1. Genes Cancer 8, 762–770. https://doi.org/10.18632/genesandcancer.159.
- Herrero-Martin, D., Osuna, D., Ordonez, J.L., Sevillano, V., Martins, A.S., Mackintosh, C., Campos, M., Madoz-Gurpide, J., Otero-Motta, A.P., Caballero, G., et al. (2009). Stable interference of EWS-FLI1 in an Ewing sarcoma cell line impairs IGF-1/IGF-1R signalling and reveals TOPK as a new target. Br. J. Cancer. 101, 80–90. https://doi.org/10.1038/sj.bjc. 6605104
- Scotlandi, K., Benini, S., Nanni, P., Lollini, P.L., Nicoletti, G., Landuzzi, L., Serra, M., Manara, M.C., Picci, P., and Baldini, N. (1998). Blockage of insulin-like growth factor-I receptor inhibits the growth of Ewing's sarcoma in athymic mice. Cancer Res. 58, 4127–4131.
- Amin, H.M., Morani, A.C., Daw, N.C., Lamhamedi-Cherradi, S.E., Subbiah, V., Menegaz, B.A., Vishwamitra, D., Eskandari, G., George, B., Benjamin, R.S., et al. (2020). IGF-1R/mTOR Targeted Therapy for Ewing Sarcoma: A Meta-Analysis of Five IGF-1R-Related Trials Matched to Proteomic and Radiologic Predictive Biomarkers. Cancers 12, 1768. https://doi.org/10.3390/cancers12071768.
- Juergens, H., Daw, N.C., Geoerger, B., Ferrari, S., Villarroel, M., Aerts, I., Whelan, J., Dirksen, U., Hixon, M.L., Yin, D., et al. (2011). Preliminary efficacy of the anti-insulin-like growth factor type 1 receptor antibody figitumumab in patients with refractory Ewing sarcoma. J. Clin. Oncol. 29, 4534–4540. https://doi.org/10.1200/JCO.2010.33.0670.
- Pappo, A.S., Patel, S.R., Crowley, J., Reinke, D.K., Kuenkele, K.P., Chawla, S.P., Toner, G.C., Maki, R.G., Meyers, P.A., Chugh, R., et al. (2011). R1507, a monoclonal antibody to the insulin-like growth factor 1 receptor, in patients with recurrent or refractory Ewing sarcoma family of tumors: results of a phase II Sarcoma Alliance for Research through Collaboration study. J. Clin. Oncol. 29, 4541–4547. https://doi.org/10.1200/JCO.2010.34.0000.
- Garofalo, C., Manara, M.C., Nicoletti, G., Marino, M.T., Lollini, P.L., Astolfi, A., Pandini, G., López-Guerrero, J.A., Schaefer, K.L., Belfiore, A., et al. (2011). Efficacy of and resistance to anti-IGF-1R therapies in Ewing's sarcoma is dependent on insulin receptor signaling. Oncogene 30, 2730–2740. https://doi.org/10.1038/onc.2010.640.
- Riggi, N., Cironi, L., Provero, P., Suvà, M.L., Kaloulis, K., Garcia-Echeverria, C., Hoffmann, F., Trumpp, A., and Stamenkovic, I. (2005). Development of Ewing's sarcoma from primary bone marrow-derived mesenchymal progenitor cells. Cancer Res. 65, 11459–11468. https://doi.org/10.1158/ 0008-5472.CAN-05-1696.

Article



- Riggi, N., Suvà, M.L., De Vito, C., Provero, P., Stehle, J.C., Baumer, K., Cironi, L., Janiszewska, M., Petricevic, T., Suvà, D., et al. (2010). EWS-FLI-1 modulates miRNA145 and SOX2 expression to initiate mesenchymal stem cell reprogramming toward Ewing sarcoma cancer stem cells. Genes Dev. 24, 916–932. https://doi.org/10.1101/gad.1899710.
- Tirode, F., Laud-Duval, K., Prieur, A., Delorme, B., Charbord, P., and Delattre, O. (2007). Mesenchymal stem cell features of Ewing tumors. Cancer. Cell. 11, 421–429. https://doi.org/10.1016/j.ccr.2007.02.027.
- von Levetzow, C., Jiang, X., Gwye, Y., von Levetzow, G., Hung, L., Cooper, A., Hsu, J.H.R., and Lawlor, E.R. (2011). Modeling initiation of Ewing sarcoma in human neural crest cells. PLoS One 6, e19305. https://doi.org/10.1371/journal.pone.0019305.
- Lin, P.P., Pandey, M.K., Jin, F., Xiong, S., Deavers, M., Parant, J.M., and Lozano, G. (2008). EWS-FLI1 induces developmental abnormalities and accelerates sarcoma formation in a transgenic mouse model. Cancer Res. 68, 8968–8975. https://doi.org/10.1158/0008-5472.CAN-08-0573.
- Brohl, A.S., Solomon, D.A., Chang, W., Wang, J., Song, Y., Sindiri, S., Patidar, R., Hurd, L., Chen, L., Shern, J.F., et al. (2014). The Genomic Landscape of the Ewing Sarcoma Family of Tumors Reveals Recurrent STAG2 Mutation. PLoS Genet. 10, e1004475. https://doi.org/10.1371/journal.pgen.1004475.
- Crompton, B.D., Stewart, C., Taylor-Weiner, A., Alexe, G., Kurek, K.C., Calicchio, M.L., Kiezun, A., Carter, S.L., Shukla, S.A., Mehta, S.S., et al. (2014). The genomic landscape of pediatric Ewing sarcoma. Cancer Discov. 4, 1326–1341. https://doi.org/10.1158/2159-8290.CD-13-1037.
- Tirode, F., Surdez, D., Ma, X., Parker, M., Le Deley, M.C., Bahrami, A., Zhang, Z., Lapouble, E., Grossetête-Lalami, S., Rusch, M., et al. (2014). Genomic landscape of Ewing sarcoma defines an aggressive subtype with co-association of STAG2 and TP53 mutations. Cancer Discov. 4, 1342–1353. https://doi.org/10.1158/2159-8290.CD-14-0622.
- Garcia, J.M., Merriam, G.R., and Kargi, A.Y. (2000). Growth Hormone in Aging. In Endotext, K.R. Feingold, B. Anawalt, A. Boyce, G. Chrousos, W.W. de Herder, K. Dhatariya, K. Dungan, J.M. Hershman, J. Hofland, and S. Kalra, eds. https://www.ncbi.nlm.nih.gov/books/NBK279163/.
- Olarescu, N.C., Gunawardane, K., Hansen, T.K., Moller, N., and Jorgensen, J.O.L. (2000). Normal Physiology of Growth Hormone in Adults. In Endotext, K.R. Feingold, B. Anawalt, A. Boyce, G. Chrousos, W.W. de Herder, K. Dhatariya, K. Dungan, J.M. Hershman, J. Hofland, and S. Kalra, eds. https://www.ncbi.nlm.nih.gov/books/NBK279056/.
- Criscitiello, C., Viale, G., Gelao, L., Esposito, A., De Laurentiis, M., De Placido, S., Santangelo, M., Goldhirsch, A., and Curigliano, G. (2015). Crosstalk between bone niche and immune system: osteoimmunology signaling as a potential target for cancer treatment. Cancer Treat Rev. 41, 61–68. https://doi.org/10.1016/j.ctrv.2014.12.001.
- Shiozawa, Y., Eber, M.R., Berry, J.E., and Taichman, R.S. (2015). Bone marrow as a metastatic niche for disseminated tumor cells from solid tumors. BoneKEy Rep. 4, 689. https://doi.org/10.1038/bonekey.2015.57.
- Hilmi, C., Larribere, L., Giuliano, S., Bille, K., Ortonne, J.P., Ballotti, R., and Bertolotto, C. (2008). IGF1 promotes resistance to apoptosis in melanoma cells through an increased expression of BCL2, BCL-X(L), and survivin. J. Invest. Dermatol. 128, 1499–1505. https://doi.org/10.1038/ sj.jid.5701185.
- Crossland, H., Kazi, A.A., Lang, C.H., Timmons, J.A., Pierre, P., Wilkinson, D.J., Smith, K., Szewczyk, N.J., and Atherton, P.J. (2013). Focal adhesion kinase is required for IGF-I-mediated growth of skeletal muscle cells via a TSC2/mTOR/S6K1-associated pathway. Am. J. Physiol. Endocrinol. Metab. 305, E183–E193. https://doi.org/10.1152/ajpendo.00541.2012.
- Reijnders, C.M.A., Bravenboer, N., Holzmann, P.J., Bhoelan, F., Blankenstein, M.A., and Lips, P. (2007). In vivo mechanical loading modulates insulin-like growth factor binding protein-2 gene expression in rat osteocytes. Calcif. Tissue Int. 80, 137–143. https://doi.org/10.1007/s00223-006-0077-4.

- Torchia, E.C., Boyd, K., Rehg, J.E., Qu, C., and Baker, S.J. (2007). EWS/ FLI-1 induces rapid onset of myeloid/erythroid leukemia in mice. Mol. Cell Biol. 27, 7918–7934. https://doi.org/10.1128/MCB.00099-07.
- Logan, M., Martin, J.F., Nagy, A., Lobe, C., Olson, E.N., and Tabin, C.J. (2002). Expression of Cre Recombinase in the developing mouse limb bud driven by a Prxl enhancer. Genesis 33, 77–80. https://doi.org/10. 1002/gene.10092.
- Love, M.I., Huber, W., and Anders, S. (2014). Moderated estimation of fold change and dispersion for RNA-seq data with DESeq2. Genome Biol. 15, 550. https://doi.org/10.1186/s13059-014-0550-8.
- Boulay, G., Sandoval, G.J., Riggi, N., Iyer, S., Buisson, R., Naigles, B., Awad, M.E., Rengarajan, S., Volorio, A., McBride, M.J., et al. (2017). Cancer-Specific Retargeting of BAF Complexes by a Prion-like Domain. Cellule 171, 163–178.e19. https://doi.org/10.1016/j.cell.2017.07.036.
- Guillon, N., Tirode, F., Boeva, V., Zynovyev, A., Barillot, E., and Delattre, O. (2009). The oncogenic EWS-FLI1 protein binds in vivo GGAA microsatellite sequences with potential transcriptional activation function. PLoS One 4, e4932. https://doi.org/10.1371/journal.pone.0004932.
- Corces, M.R., Trevino, A.E., Hamilton, E.G., Greenside, P.G., Sinnott-Armstrong, N.A., Vesuna, S., Satpathy, A.T., Rubin, A.J., Montine, K.S., Wu, B., et al. (2017). An improved ATAC-seq protocol reduces background and enables interrogation of frozen tissues. Nat. Methods 14, 959–962. https://doi.org/10.1038/nmeth.4396.
- Korotkevich, G., Sukhov, V., Budin, N., Shpak, B., Artyomov, M.N., and Sergushichev, A. (2021). Fast gene set enrichment analysis. bioRxiv, 060012. https://doi.org/10.1101/060012.
- Mancarella, C., and Scotlandi, K. (2018). IGF system in sarcomas: a crucial pathway with many unknowns to exploit for therapy. J. Mol. Endocrinol. 61, T45–T60. https://doi.org/10.1530/JME-17-0250.
- Juul, A., Bang, P., Hertel, N.T., Main, K., Dalgaard, P., Jørgensen, K., Müller, J., Hall, K., and Skakkebaek, N.E. (1994). Serum insulin-like growth factor-I in 1030 healthy children, adolescents, and adults: relation to age, sex, stage of puberty, testicular size, and body mass index. J. Clin. Endocrinol. Metab. 78, 744–752. https://doi.org/10.1210/jcem. 78.3.8126152.
- Juul, A., and Skakkebæk, N.E. (2019). Why Do Normal Children Have Acromegalic Levels of IGF-I During Puberty? J. Clin. Endocrinol. Metab. 104, 2770–2776. https://doi.org/10.1210/jc.2018-02099.
- Honegger, A., and Humbel, R.E. (1986). Insulin-like growth factors I and II in fetal and adult bovine serum. Purification, primary structures, and immunological cross-reactivities. J. Biol. Chem. 261, 569–575.
- Garcia-Echeverria, C., Pearson, M.A., Marti, A., Meyer, T., Mestan, J., Zimmermann, J., Gao, J., Brueggen, J., Capraro, H.G., Cozens, R., et al. (2004). In vivo antitumor activity of NVP-AEW541-A novel, potent, and selective inhibitor of the IGF-IR kinase. Cancer Cell 5, 231–239. https://doi.org/10.1016/s1535-6108(04)00051-0.
- Scotlandi, K., Manara, M.C., Nicoletti, G., Lollini, P.L., Lukas, S., Benini, S., Croci, S., Perdichizzi, S., Zambelli, D., Serra, M., et al. (2005). Antitumor activity of the insulin-like growth factor-I receptor kinase inhibitor NVP-AEW541 in musculoskeletal tumors. Cancer Res. 65, 3868–3876. https://doi.org/10.1158/0008-5472.CAN-04-3192.
- Fornes, O., Castro-Mondragon, J.A., Khan, A., van der Lee, R., Zhang, X., Richmond, P.A., Modi, B.P., Correard, S., Gheorghe, M., Baranašić, D., et al. (2020). JASPAR 2020: update of the open-access database of transcription factor binding profiles. Nucleic Acids Res. 48, D87–D92. https://doi.org/10.1093/nar/gkz1001.
- 51. Surdez, D., Benetkiewicz, M., Perrin, V., Han, Z.Y., Pierron, G., Ballet, S., Lamoureux, F., Rédini, F., Decouvelaere, A.V., Daudigeos-Dubus, E., et al. (2012). Targeting the EWSR1-FLI1 oncogene-induced protein kinase PKC-beta abolishes ewing sarcoma growth. Cancer Res. 72, 4494–4503. https://doi.org/10.1158/0008-5472.CAN-12-0371.
- Orth, M.F., Hölting, T.L.B., Dallmayer, M., Wehweck, F.S., Paul, T., Musa, J., Baldauf, M.C., Surdez, D., Delattre, O., Knott, M.M.L., et al. (2020).





- High Specificity of BCL11B and GLG1 for EWSR1-FLI1 and EWSR1-ERG Positive Ewing Sarcoma. Cancers 12, 644. https://doi.org/10.3390/cancers12030644.
- Wiles, E.T., Lui-Sargent, B., Bell, R., and Lessnick, S.L. (2013). BCL11B is up-regulated by EWS/FLI and contributes to the transformed phenotype in Ewing sarcoma. PLoS One 8, e59369. https://doi.org/10.1371/journal. pone.0059369.
- Ren, C., Ren, T., Yang, K., Wang, S., Bao, X., Zhang, F., and Guo, W. (2016). Inhibition of SOX2 induces cell apoptosis and G1/S arrest in Ewing's sarcoma through the PI3K/Akt pathway. J. Exp. Clin. Cancer Res. 35, 44. https://doi.org/10.1186/s13046-016-0321-3.
- Sannino, G., Marchetto, A., Ranft, A., Jabar, S., Zacherl, C., Alba-Rubio, R., Stein, S., Wehweck, F.S., Kiran, M.M., Hölting, T.L.B., et al. (2019). Gene expression and immunohistochemical analyses identify SOX2 as major risk factor for overall survival and relapse in Ewing sarcoma patients. EBioMedicine 47, 156–162. https://doi.org/10.1016/j.ebiom. 2019.08.002.
- Ioannidis, P., Trangas, T., Dimitriadis, E., Samiotaki, M., Kyriazoglou, I., Tsiapalis, C.M., Kittas, C., Agnantis, N., Nielsen, F.C., Nielsen, J., et al. (2001). C-MYC and IGF-II mRNA-binding protein (CRD-BP/IMP-1) in benign and malignant mesenchymal tumors. Int. J. Cancer 94, 480–484. https://doi.org/10.1002/ijc.1512.
- Vormoor, B., and Curtin, N.J. (2014). Poly(ADP-ribose) polymerase inhibitors in Ewing sarcoma. Curr. Opin. Oncol. 26, 428–433. https://doi.org/10.1097/CCO.0000000000000091.
- Okada, M., Cheeseman, I.M., Hori, T., Okawa, K., McLeod, I.X., Yates, J.R., 3rd, Desai, A., and Fukagawa, T. (2006). The CENP-H-I complex is required for the efficient incorporation of newly synthesized CENP-A into centromeres. Nat. Cell Biol. 8, 446–457. https://doi.org/10.1038/ ncb1396.
- Shirakawa, J., Fernandez, M., Takatani, T., El Ouaamari, A., Jungtrakoon, P., Okawa, E.R., Zhang, W., Yi, P., Doria, A., and Kulkarni, R.N. (2017). Insulin Signaling Regulates the FoxM1/PLK1/CENP-A Pathway to Promote Adaptive Pancreatic beta Cell Proliferation. Cell Metab. 25, 868–882.e5. https://doi.org/10.1016/j.cmet.2017.02.004.
- Magro, G., Salvatorelli, L., Alaggio, R., D'Agata, V., Nicoletti, F., Di Cataldo, A., and Parenti, R. (2017). Diagnostic utility of cyclin D1 in the diagnosis of small round blue cell tumors in children and adolescents. Hum. Pathol. 60, 58–65. https://doi.org/10.1016/j.humpath.2016.07.038.
- 61. Kaneda, A., Seike, T., Danjo, T., Nakajima, T., Otsubo, N., Yamaguchi, D., Tsuji, Y., Hamaguchi, K., Yasunaga, M., Nishiya, Y., et al. (2020). The novel potent TEAD inhibitor, K-975, inhibits YAP1/TAZ-TEAD protein-protein interactions and exerts an anti-tumor effect on malignant pleural mesothelioma. Am. J. Cancer Res. 10, 4399–4415.
- Langen, U.H., Pitulescu, M.E., Kim, J.M., Enriquez-Gasca, R., Sivaraj, K.K., Kusumbe, A.P., Singh, A., Di Russo, J., Bixel, M.G., Zhou, B., et al. (2017). Cell-matrix signals specify bone endothelial cells during developmental osteogenesis. Nat. Cell Biol. 19, 189–201. https://doi. org/10.1038/ncb3476.
- Leacock, S.W., Basse, A.N., Chandler, G.L., Kirk, A.M., Rakheja, D., and Amatruda, J.F. (2012). A zebrafish transgenic model of Ewing's sarcoma reveals conserved mediators of EWS-FLI1 tumorigenesis. Dis. Model. Mech. 5, 95–106. https://doi.org/10.1242/dmm.007401.
- Bogin, B. (1999). Evolutionary perspective on human growth. Annu. Rev. Anthropol. 28, 109–153. https://doi.org/10.1146/annurev.anthro. 28.1.109.
- Powell-Braxton, L., Hollingshead, P., Giltinan, D., Pitts-Meek, S., and Stewart, T. (1993). Inactivation of the IGF-I gene in mice results in perinatal lethality. Ann. N. Y. Acad. Sci. 692, 300–301. https://doi.org/10. 1111/j.1749-6632.1993.tb26240.x.
- 66. Sjogren, K., Liu, J.L., Blad, K., Skrtic, S., Vidal, O., Wallenius, V., LeRoith, D., Tornell, J., Isaksson, O.G., Jansson, J.O., and Ohlsson, C. (1999). Liver-derived insulin-like growth factor I (IGF-I) is the principal source of IGF-I in blood but is not required for postnatal body growth in mice.

- Proc. Natl. Acad. Sci. USA 96, 7088–7092. https://doi.org/10.1073/pnas.96.12.7088.
- 67. Miura, M., Miura, Y., Padilla-Nash, H.M., Molinolo, A.A., Fu, B., Patel, V., Seo, B.M., Sonoyama, W., Zheng, J.J., Baker, C.C., et al. (2006). Accumulated chromosomal instability in murine bone marrow mesenchymal stem cells leads to malignant transformation. Stem Cell. 24, 1095–1103. https://doi.org/10.1634/stemcells.2005-0403.
- Zhou, Y.F., Bosch-Marce, M., Okuyama, H., Krishnamachary, B., Kimura, H., Zhang, L., Huso, D.L., and Semenza, G.L. (2006). Spontaneous transformation of cultured mouse bone marrow-derived stromal cells. Cancer Res. 66, 10849–10854. https://doi.org/10.1158/0008-5472. CAN-06-2146.
- Vasileva, E., Warren, M., Triche, T.J., and Amatruda, J.F. (2022). Dysregulated heparan sulfate proteoglycan metabolism promotes Ewing sarcoma tumor growth. Elife 11, e69734. https://doi.org/10.7554/eLife.60734
- Kehr, S., Haydn, T., Bierbrauer, A., Irmer, B., Vogler, M., and Fulda, S. (2020). Targeting BCL-2 proteins in pediatric cancer: Dual inhibition of BCL-XL and MCL-1 leads to rapid induction of intrinsic apoptosis. Cancer Lett. 482, 19–32. https://doi.org/10.1016/j.canlet.2020.02.041.
- Tsafou, K., Katschnig, A.M., Radic-Sarikas, B., Mutz, C.N., Iljin, K., Schwentner, R., Kauer, M.O., Mühlbacher, K., Aryee, D.N.T., Westergaard, D., et al. (2018). Identifying the druggable interactome of EWS-FLI1 reveals MCL-1 dependent differential sensitivities of Ewing sarcoma cells to apoptosis inducers. Oncotarget 9, 31018–31031. https://doi.org/ 10.18632/oncotarget.25760.
- Hakuno, F., and Takahashi, S.I. (2018). IGF1 receptor signaling pathways. J. Mol. Endocrinol. 61, T69–T86. https://doi.org/10.1530/JME-17-0311.
- Pietruczuk, P., Jain, A., Simo-Cheyou, E.R., Anand-Srivastava, M.B., and Srivastava, A.K. (2019). Protein kinase B/AKT mediates insulin-like growth factor 1-induced phosphorylation and nuclear export of histone deacetylase 5 via NADPH oxidase 4 activation in vascular smooth muscle cells. J. Cell. Physiol. 234, 17337–17350. https://doi.org/10.1002/jcp. 28353.
- Warsito, D., Lin, Y., Gnirck, A.C., Sehat, B., and Larsson, O. (2016). Nuclearly translocated insulin-like growth factor 1 receptor phosphorylates histone H3 at tyrosine 41 and induces SNAI2 expression via Brg1 chromatin remodeling protein. Oncotarget 7, 42288–42302. https://doi.org/10.18632/oncotarget.9785.
- Aleksic, T., Gray, N., Wu, X., Rieunier, G., Osher, E., Mills, J., Verrill, C., Bryant, R.J., Han, C., Hutchinson, K., et al. (2018). Nuclear IGF1R Interacts with Regulatory Regions of Chromatin to Promote RNA Polymerase II Recruitment and Gene Expression Associated with Advanced Tumor Stage. Cancer Res. 78, 3497–3509. https://doi.org/10.1158/0008-5472. CAN-17-3498.
- Quagliarini, F., Mir, A.A., Balazs, K., Wierer, M., Dyar, K.A., Jouffe, C., Makris, K., Hawe, J., Heinig, M., Filipp, F.V., et al. (2019). Cistromic Reprogramming of the Diurnal Glucocorticoid Hormone Response by High-Fat Diet. Mol. Cell 76, 531–545.e5. https://doi.org/10.1016/j.molcel.2019.10.007.
- Srivastava, S., Nataraj, N.B., Sekar, A., Ghosh, S., Bornstein, C., Drago-Garcia, D., Roth, L., Romaniello, D., Marrocco, I., David, E., et al. (2019).
 ETS Proteins Bind with Glucocorticoid Receptors: Relevance for Treatment of Ewing Sarcoma. Cell Rep. 29, 104–117.e4. https://doi.org/10.1016/j.celrep.2019.08.088.
- Kim, S.L., Choi, H.S., Kim, J.H., and Lee, D.S. (2020). The Antiasthma Medication Ciclesonide Suppresses Breast Cancer Stem Cells through Inhibition of the Glucocorticoid Receptor Signaling-Dependent YAP Pathway. Molecules 25, 6028. https://doi.org/10.3390/molecules25246028.
- Sorrentino, G., Ruggeri, N., Zannini, A., Ingallina, E., Bertolio, R., Marotta, C., Neri, C., Cappuzzello, E., Forcato, M., Rosato, A., et al. (2017). Glucocorticoid receptor signalling activates YAP in breast cancer. Nat. Commun. 8, 14073. https://doi.org/10.1038/ncomms14073.

Article



- Straßburger, K., Tiebe, M., Pinna, F., Breuhahn, K., and Teleman, A.A. (2012). Insulin/IGF signaling drives cell proliferation in part via Yorkie/YAP. Dev. Biol. 367, 187–196. https://doi.org/10.1016/j.ydbio.2012.05.008.
- Zhu, H., Wang, D.D., Yuan, T., Yan, F.J., Zeng, C.M., Dai, X.Y., Chen, Z.B., Chen, Y., Zhou, T., Fan, G.H., et al. (2018). Multikinase Inhibitor CT-707 Targets Liver Cancer by Interrupting the Hypoxia-Activated IGF-1R-YAP Axis. Cancer Res. 78, 3995–4006. https://doi.org/10.1158/0008-5472.CAN-17-1548.
- Zhou, X., Chen, N., Xu, H., Zhou, X., Wang, J., Fang, X., Zhang, Y., Li, Y., Yang, J., and Wang, X. (2020). Regulation of Hippo-YAP signaling by insulin-like growth factor-1 receptor in the tumorigenesis of diffuse large B-cell lymphoma. J. Hematol. Oncol. 13, 77. https://doi.org/10.1186/s13045-020-00906-1.
- Borreguero-Munoz, N., Fletcher, G.C., Aguilar-Aragon, M., Elbediwy, A., Vincent-Mistiaen, Z.I., and Thompson, B.J. (2019). The Hippo pathway integrates PI3K-Akt signals with mechanical and polarity cues to control tissue growth. PLoS Biol. 17, e3000509. https://doi.org/10.1371/journal. pbio.3000509.
- 84. Laperle, A., Hsiao, C., Lampe, M., Mortier, J., Saha, K., Palecek, S.P., and Masters, K.S. (2015). alpha-5 Laminin Synthesized by Human Pluripotent Stem Cells Promotes Self-Renewal. Stem Cell Rep. 5, 195–206. https://doi.org/10.1016/j.stemcr.2015.06.009.
- Yu, K.R., Yang, S.R., Jung, J.W., Kim, H., Ko, K., Han, D.W., Park, S.B., Choi, S.W., Kang, S.K., Schöler, H., and Kang, K.S. (2012). CD49f enhances multipotency and maintains stemness through the direct regulation of OCT4 and SOX2. Stem Cell. 30, 876–887. https://doi.org/10.1002/stem.1052.
- Zhi, X., Zhao, D., Zhou, Z., Liu, R., and Chen, C. (2012). YAP promotes breast cell proliferation and survival partially through stabilizing the KLF5 transcription factor. Am. J. Pathol. 180, 2452–2461. https://doi. org/10.1016/j.ajpath.2012.02.025.
- Christensen, L., Joo, J., Lee, S., Wai, D., Triche, T.J., and May, W.A. (2013). FOXM1 is an oncogenic mediator in Ewing Sarcoma. PLoS One 8, e54556. https://doi.org/10.1371/journal.pone.0054556.
- Fernandez-L, A., Northcott, P.A., Dalton, J., Fraga, C., Ellison, D., Angers, S., Taylor, M.D., and Kenney, A.M. (2009). YAP1 is amplified and upregulated in hedgehog-associated medulloblastomas and mediates Sonic hedgehog-driven neural precursor proliferation. Genes Dev. 23, 2729–2741. https://doi.org/10.1101/gad.1824509.
- Dai, H., Shao, Y.W., Tong, X., Wu, X., Pang, J., Feng, A., and Yang, Z. (2020). YAP1 amplification as a prognostic factor of definitive chemora-diotherapy in nonsurgical esophageal squamous cell carcinoma. Cancer Med. 9, 1628–1637. https://doi.org/10.1002/cam4.2761.
- Niu, G., Bak, A., Nusselt, M., Zhang, Y., Pausch, H., Flisikowska, T., Schnieke, A.E., and Flisikowski, K. (2021). Allelic Expression Imbalance Analysis Identified YAP1 Amplification in p53- Dependent Osteosarcoma. Cancers 13, 1364. https://doi.org/10.3390/cancers13061364.
- Zender, L., Spector, M.S., Xue, W., Flemming, P., Cordon-Cardo, C., Silke, J., Fan, S.T., Luk, J.M., Wigler, M., Hannon, G.J., et al. (2006). Identification and validation of oncogenes in liver cancer using an integrative oncogenomic approach. Cell 125, 1253–1267. https://doi.org/10.1016/j.cell.2006.05.030.
- Ma, O., Cai, W.W., Zender, L., Dayaram, T., Shen, J., Herron, A.J., Lowe, S.W., Man, T.K., Lau, C.C., and Donehower, L.A. (2009). MMP13, Birc2 (cIAP1), and Birc3 (cIAP2), amplified on chromosome 9, collaborate with p53 deficiency in mouse osteosarcoma progression. Cancer Res. 69, 2559–2567. https://doi.org/10.1158/0008-5472.CAN-08-2929.
- Kapoor, A., Yao, W., Ying, H., Hua, S., Liewen, A., Wang, Q., Zhong, Y., Wu, C.J., Sadanandam, A., Hu, B., et al. (2014). Yap1 activation enables bypass of oncogenic Kras addiction in pancreatic cancer. Cell 158, 185–197. https://doi.org/10.1016/j.cell.2014.06.003.
- 94. Tao, L., Xiang, D., Xie, Y., Bronson, R.T., and Li, Z. (2017). Induced p53 loss in mouse luminal cells causes clonal expansion and development

- of mammary tumours. Nat. Commun. 8, 14431. https://doi.org/10.1038/ncomms14431.
- Shih, D.J.H., Nayyar, N., Bihun, I., Dagogo-Jack, I., Gill, C.M., Aquilanti, E., Bertalan, M., Kaplan, A., D'Andrea, M.R., Chukwueke, U., et al. (2020). Genomic characterization of human brain metastases identifies drivers of metastatic lung adenocarcinoma. Nat. Genet. 52, 371–377. https://doi. org/10.1038/s41588-020-0592-7.
- Rodriguez-Nunez, P., Romero-Perez, L., Amaral, A.T., Puerto-Camacho, P., Jordan, C., Marcilla, D., Grunewald, T.G., Alonso, J., de Alava, E., and Diaz-Martin, J. (2020). Hippo pathway effectors YAP1/TAZ induce an EWS-FLI1-opposing gene signature and associate with disease progression in Ewing sarcoma. J. Pathol. 250, 374–386. https://doi.org/10.1002/path.5379.
- Bierbaumer, L., Katschnig, A.M., Radic-Sarikas, B., Kauer, M.O., Petro, J.A., Högler, S., Gurnhofer, E., Pedot, G., Schäfer, B.W., Schwentner, R., et al. (2021). YAP/TAZ inhibition reduces metastatic potential of Ewing sarcoma cells. Oncogenesis 10, 2. https://doi.org/10.1038/s41389-020-00294-8.
- Kovar, H., Bierbaumer, L., and Radic-Sarikas, B. (2020). The YAP/TAZ Pathway in Osteogenesis and Bone Sarcoma Pathogenesis. Cells 9, 972. https://doi.org/10.3390/cells9040972.
- Katschnig, A.M., Kauer, M.O., Schwentner, R., Tomazou, E.M., Mutz, C.N., Linder, M., Sibilia, M., Alonso, J., Aryee, D.N.T., and Kovar, H. (2017). EWS-FLI1 perturbs MRTFB/YAP-1/TEAD target gene regulation inhibiting cytoskeletal autoregulatory feedback in Ewing sarcoma. Oncogene 36, 5995–6005. https://doi.org/10.1038/onc.2017.202.
- Barry, E.R., Simov, V., Valtingojer, I., and Venier, O. (2021). Recent Therapeutic Approaches to Modulate the Hippo Pathway in Oncology and Regenerative Medicine. Cells 10, 2715. https://doi.org/10.3390/cells10102715.
- 101. Otsuki, H., Uemori, T., Inai, Y., Suzuki, Y., Araki, T., Nan-Ya, K.I., and Yoshinari, K. (2024). Reversible and monitorable nephrotoxicity in rats by the novel potent transcriptional enhanced associate domain (TEAD) inhibitor, K-975. J. Toxicol. Sci. 49, 175–191. https://doi.org/10.2131/jts.49.175.
- Federico, A., and Monti, S. (2020). hypeR: an R package for geneset enrichment workflows. Bioinformatics 36, 1307–1308. https://doi.org/ 10.1093/bioinformatics/btz700.
- 103. Smith, J.P., Corces, M.R., Xu, J., Reuter, V.P., Chang, H.Y., and Sheffield, N.C. (2021). PEPATAC: an optimized pipeline for ATAC-seq data analysis with serial alignments. NAR Genom. Bioinform. 3, Iqab101. https://doi.org/10.1093/nargab/Iqab101.
- 104. Zhang, Y., Liu, T., Meyer, C.A., Eeckhoute, J., Johnson, D.S., Bernstein, B.E., Nusbaum, C., Myers, R.M., Brown, M., Li, W., and Liu, X.S. (2008). Model-based analysis of ChIP-Seq (MACS). Genome Biol. 9, R137. https://doi.org/10.1186/gb-2008-9-9-r137.
- Schneider, C.A., Rasband, W.S., and Eliceiri, K.W. (2012). NIH Image to ImageJ (2012): 25 years of image analysis. Nat. Methods 9, 671–675. https://doi.org/10.1038/nmeth.2089.
- Bliss, C.I. (1939). THE TOXICITY OF POISONS APPLIED JOINTLY1. Ann. Appl. Biol. 26, 585–615.
- 107. Webb, J.L. (1963). Enzyme and Metabolic Inhibitors, 1 (Academic Press).
- 108. Ewels, P.A., Peltzer, A., Fillinger, S., Patel, H., Alneberg, J., Wilm, A., Garcia, M.U., Di Tommaso, P., and Nahnsen, S. (2020). The nf-core framework for community-curated bioinformatics pipelines. Nat. Biotechnol. 38, 276–278. https://doi.org/10.1038/s41587-020-0439-x.
- 109. Kuleshov, M.V., Jones, M.R., Rouillard, A.D., Fernandez, N.F., Duan, Q., Wang, Z., Koplev, S., Jenkins, S.L., Jagodnik, K.M., Lachmann, A., et al. (2016). Enrichr: a comprehensive gene set enrichment analysis web server 2016 update. Nucleic Acids Res. 44, W90–W97. https://doi.org/10.1093/nar/gkw377.
- Kinsey, M., Smith, R., and Lessnick, S.L. (2006). NR0B1 is required for the oncogenic phenotype mediated by EWS/FLI in Ewing's sarcoma. Mol.





- Cancer Res. 4, 851–859. https://doi.org/10.1158/1541-7786.MCR-06-0090.
- 111. Riggi, N., Suvà, M.L., Suvà, D., Cironi, L., Provero, P., Tercier, S., Joseph, J.M., Stehle, J.C., Baumer, K., Kindler, V., and Stamenkovic, I. (2008). EWS-FLI-1 expression triggers a Ewing's sarcoma initiation program in primary human mesenchymal stem cells. Cancer Res. 68, 2176–2185. https://doi.org/10.1158/0008-5472.CAN-07-1761.
- 112. Subramanian, A., Tamayo, P., Mootha, V.K., Mukherjee, S., Ebert, B.L., Gillette, M.A., Paulovich, A., Pomeroy, S.L., Golub, T.R., Lander, E.S., and Mesirov, J.P. (2005). Gene set enrichment analysis: a knowledge-based approach for interpreting genome-wide expression profiles. Proc. Natl. Acad. Sci. USA 102, 15545–15550. https://doi.org/10.1073/pnas.0506580102.
- 113. Liao, Y., Smyth, G.K., and Shi, W. (2019). The R package Rsubread is easier, faster, cheaper and better for alignment and quantification of

- RNA sequencing reads. Nucleic Acids Res. 47, e47. https://doi.org/10.1093/nar/gkz114.
- 114. Castro-Mondragon, J.A., Riudavets-Puig, R., Rauluseviciute, I., Lemma, R.B., Turchi, L., Blanc-Mathieu, R., Lucas, J., Boddie, P., Khan, A., Manosalva Pérez, N., et al. (2022). JASPAR 2022: the 9th release of the openaccess database of transcription factor binding profiles. Nucleic Acids Res. 50, D165–D173. https://doi.org/10.1093/nar/gkab1113.
- 115. Garcia, M., Juhos, S., Larsson, M., Olason, P.I., Martin, M., Eisfeldt, J., DiLorenzo, S., Sandgren, J., Díaz De Ståhl, T., Ewels, P., et al. (2020). Sarek: A portable workflow for whole-genome sequencing analysis of germline and somatic variants. F1000Res. 9, 63. https://doi.org/10.12688/f1000research.16665.2.
- 116. Talevich, E., Shain, A.H., Botton, T., and Bastian, B.C. (2016). CNVkit: Genome-Wide Copy Number Detection and Visualization from Targeted DNA Sequencing. PLoS Comput. Biol. 12, e1004873. https://doi.org/10. 1371/journal.pcbi.1004873.



STAR***METHODS**

KEY RESOURCES TABLE

REAGENT or RESOURCE	SOURCE	IDENTIFIER
Antibodies		
Anti-digoxigenin-alkaline phosphatase	Roche	Cat# 11093274910; RRID:AB_514497
AKT	Cell Signaling Technology	Cat# 4685; RRID:AB_2225340
B-Actin	Abcam	Cat# ab20272; RRID:AB_445482
CD90-2-APC	BD Pharmingen	Cat# 561974; RRID:AB_10895115
CD44-PE	BD Pharmingen	Cat# 561860; RRID:AB_10895375
CD45-APC	BD Pharmingen	Cat# 559864; RRID:AB_398672
CD19-APC-Cy7	BD Pharmingen	Cat# 557655; RRID:AB_396770
FLI-1 (EPR4646)	Abcam	Cat# ab133485; RRID:AB_2722650
FOXM1 (EPR17379)	Abcam	Cat# ab207298; RRID:AB_3068347
GAPDH (D16H11)XP	Cell Signaling Technology	Cat# 5174; RRID:AB_10622025
HA tag (6E2)	Cell Signaling Technology	Cat# 2367; RRID:AB_10691311
IGF1R	Cell Signaling Technology	Cat# 3027; RRID:AB_2122378
KLF5	Abcam	Cat# ab137676; RRID:AB_2744553
Laminin alpha 5/LAMA5 antibody [EPR18919]	Abcam	Cat# ab184330;
p-Akt (Ser473) (D9E)	Cell Signaling Technology	Cat# 4060; RRID:AB_2315049
p-IGF-IR beta (Y1135/1136)/InsR beta (19H7)	Cell Signaling	Cat# 3024; RRID:AB_331253
YAP/TAZ (D24E4)	Cell Signaling Technology	Cat# 8418; RRID:AB_10950494
Chemicals, recombinant proteins, media		
Acetic anhydride	Sigma-Aldrich	Cat# 242845
Accutase	Gibco	Cat# A1110501
Alcian Blue	Sigma Aldrich	Cat# A5268-10G
Alizarin Red	Sigma-Aldrich	Cat# A5533-25g
CliniMACS buffer	Miltenyi Biotec GmbH	Cat# 130021201
Digitonin	New England Biolabs	Cat# 11175025910
Fetal Bovine Serum	Gibco	Cat# 10099158
Insuline	Sigma-Aldrich	Cat# 19278-5MI
IGF-1	ImmunoTools	Cat# 11343316
K-975	MedChemExpress	Cat# HY-138565; CAS: 2563855-03-6
Lipofectamine 2000	Invitrogen/ThermoFisher	Cat# 11668019
NVP-AEW541	MedChemExpress	Cat# HY-50866; CAS: 475489-16-8
Oligofectamine reagent	Invitrogen/ThermoFisher Scientific	Cat# 58303
Polybrene	Milipore/Sigma	Cat# TR-1003-G
RPMI1640	Gibco	Cat# 61870044
SeaPlaque GTG agarose	Lonza	Cat# 50111
Xylene substitute	Thermo Scientific	Cat# 9990505
Critical commercial assays		
CellTiter-Glo® Luminescent Cell Viability Assay	Promega	Cat# G7570
Illumina Tagment DNA Enzyme and Buffer Small Kit	Illumina	Cat# 20034197
LentiCRISPR Yap1 sgRNA Crispr/Cas9 all in-one lentivector set mouse	Applied Biological Materials (abm)	Cat# 505841140595
		10 11 1

(Continued on next page)



Continued		
REAGENT or RESOURCE	SOURCE	IDENTIFIER
Lenti-X Concentrator	TaKaRa	Cat# 631232
MesenCult adipogenic differentiation kit	Stem Cell Technologies	Cat# 05412
MesenCult osteogenic stimulatory kit	Stem Cell Technologies	Cat# 05504
MesenCult-ACF chondrogenic differentiation kit	Stem Cell Technologies	Cat# 05455
NEBNext® Poly(A) mRNA Magnetic Isolation Module	New England BioLabs	Cat# E7490S
ON-TARGETplus SMARTpool mouse siRNAs against Yap1	Dharmacon/Horizon	Cat# L-012200-00-0005
ON-TARGETplus non-targeting pool	Dharmacon/Horizon	Cat# D-001810-10-20
RNA DIG labelling kit	Roche	Cat# 11175025910
RNeasy Mini Kit (250)	QUIAGEN	Cat# 74106
Genomic DNA Purification Kit	Monarch	Cat# T3010S
Deposited data		
RNA-seq	This paper	GEO: GSE269006
ATAC-seq	This paper	GEO: GSE269004
Experimental Model and Study Participant Detail	ls: Cell lines	
A673	American Type Culture Collection	Cat# CRL-1598
Lenti-X293T cells	Takara	Cat# 632180
Ewing sarcoma cell line STA-ET-1	Generated in-house	STA-ET-1
Ewing sarcoma cell line SK-N-MC	June Biedler (Memorial Sloan Kettering Cancer Center (New York, USA)	SK-N-MC
EF ^{Prx1} MSCLC	This paper	N/A
hr-EF ^{Prx1} MSCLC	This paper	N/A
Experimental Model and Study Participant Detail	ls: Organisms/strains	
Cre-inducible EWS/FLI-1 mouse (Rosa26loxP-STOPloxP-HA-EF)	Suzanne Baker (St. Jude Children's Research Hospital)	Torchia et al. ³⁷
Prx1-Cre mouse	Malcolm Logan (King's College, London, UK)	Logan et al. ³⁸
SCID mice (C.B-17/Prkcdscid)	Charles River Laboratories	C.B-17/Prkcdscid
hr-EF ^{Prx1} xenografts	This paper	N/A
Oligonucleotides		
Primer: Yap1 Forward: ACCCTCGTTTTGCCATGAAC	This paper	N/A
Primer: Yap1 Reverse: TGTGCTGGGATTGATATTCCGTA	This paper	N/A
Primer: lgf2bp1 Forward: CGGCAACCTCAACGAGAGT	This paper	N/A
Primer: lgf2bp1 Reverse: GCGTAGCCGGATTTGACCAA	This paper	N/A
Primer: Hpf1 Forward: TGGGGTACTCGCTTGAACAG	This paper	N/A
Primer: Hpf1 Reverse: CAAGCCTGCACCATGAAAGG	This paper	N/A
Primer: Cenpq Forward: AATGTGCAACACTGAAAGTCCC	This paper	N/A
Primer: Cenpq Reverse: ATTCTGGTTTGGAATTAGTGCCA	This paper	N/A
Primer: Ccnd1 Forward: GCGTACCCTGACACCAATCTC	This paper	N/A

(Continued on next page)



Continued		
REAGENT or RESOURCE	SOURCE	IDENTIFIER
Primer: Ccnd1 Reverse: ACTTGAAGTAAGATACGGAGGGC	This paper	N/A
Primer: EWS::FLI1 Forward: TCCTACAGCCAAGCTCCAAGTC	This paper	N/A
Primer: EWS::FLI1 Reverse: ACTCCCCGTTGGTCCCCTCC	This paper	N/A
Primer: Lama5 Forward: CTGGCGGAGATCCCAATCAG	This paper	N/A
Primer: Lama5 Reverse: GTGTGACGTTGACCTCATTGT	This paper	N/A
Primer: Prkcb Forward: TGGATCGCTGCTGTATGGAC	This paper	N/A
Primer: Prkcb Reverse: GGCTGGGGACGTTCATCAC	This paper	N/A
Primer: RorC Forward: CGCGGAGCAGACACACTTA	This paper	N/A
Primer: RorC Reverse: CCCTGGACCTCTGTTTTGGC	This paper	N/A
Primer: Foxm1 Forward: CAGAATGCCCCGAGTGAAACA	This paper	N/A
Primer: Foxm1 Reverse: GTGGGGTGGTTGATAATCTTGAT	This paper	N/A
Primer: Yap1 Forward: ACCCTCGTTTTGCCATGAAC	This paper	N/A
Plasmids		
Sh-scr (ON-TARGETplus nontargeting siRNA pool)	Dharmacon	Cat# D-001810-10-05
psPAX2	Addgene	Cat# 12260
pMD2.G	Addgene	Cat# 12259
Plasticware		
ViewPlate-96, white with clear bottom	Perkin Elmer	Cat# 6005181
sgRNAs: see Table(sg-Yap1, sg-ctr, sg-EF,.)		
Software and algorithms		
nf-core/rnaseq pipeline	v3.14.0	https://nf-co.re/rnaseq/3.14.0
DESeq2	v1.38.3	Love et al. ³⁹
nypeR package v1.14.0	v1.14.0	Federico et al. ¹⁰²
GSEA	v1.24.0	https://github.com/ctlab/fgsea/
MSigDB		https://www.gsea-msigdb.org/).
pypiper	v0.10.0	Smith et al. 103
PEPATAC	v0.8.6	Smith et al. ¹⁰³
MACS2	v2.1.0	Zhang et al. ¹⁰⁴
R	v4.2.2	https://www.r-project.org/
GraphPad Prism	Version 8	https://www.graphpad.com
enrichR		http://amp.pharm.mssm.edu/Enrichr/
cancerbits/noorizadeh2025_ef_igf1_yap1: 2025-01-31	This paper	https://github.com/cancerbits/ noorizadeh2025_ef_igf1_yap1 https://doi.org/10.5281/zenodo.14780467
Image J	Version 1.52; Schneider et al. 105	https://imagej.net/ij/index.html
BioRender	Science Suite Inc.	https://biorender.com/





EXPERIMENTAL MODEL AND STUDY PARTICIPANT DETAILS

Genetically modified mice

Mice harboring a Cre-inducible *EF* knocked into the ubiquitous *Rosa26* locus (*Rosa26loxP-STOPloxP-HA-EF* allele) ³⁷ were crossed to a Prx1Cre line ³⁸. To determine the age of the embryos, female mice in breeding cages were daily checked for vaginal plugs. If a plug was found, the female was separated at noon and that day was counted as E (embryonic day) 0,5. Embryos were then harvested at indicated time points. Mice were kept under standard conditions at the Decentralized Biomedical Facility of the Medical University of Vienna on a 12 hours light-dark cycle. All animal experiments were approved by the Austrian ministry for science and research (license number: BMWF-66009/0139-C/GT/2007).

Cell lines

Among EwS cell lines used in this study, STA-ET-1 was established from a female patient in-house, TC32 (female) was kindly provided by Sue Burchill (University of Leeds, UK), A673 (female) and SK-N-MC (female) were from the American Type Culture Collection (CRL-1598 and HTB-10). Lenti-X293T lenti-viral packaging cells were purchased from Takara Bio (#632180). Cell lines were cultivated in RPMI1640 (#61870044, Thermo Fisher Scientific) and DMEM (#2023-09, Gibco) in the presence of 10% fetal calf serum (#10270106, Thermo Fisher Scientific). Cell lines were authenticated by STR profiling and were regularly screened for mycoplasma (Mykoalert detection kit; Lonza, Basel, Switzerland).

METHOD DETAILS

Preparation and expansion of MSCLC

Mesenchymal stem cell like cells (MSCL) from Prx1Cre founder mice used as controls were isolated by flashing the femur and tibia of P1 day old mice. To obtain the cells from cartilaginous elements of mouse EF^{Prx1} mutants, they were first cleaned from muscles and surrounding tissues, then cut in pieces and left in alpha-DMEM, 10% FCS, 0.1% Pen/Strep and 0.1% glutamine.

Skeletal staining

Embryos were skinned, eviscerated, fixed in 4% paraformaldehyde (PFA)/PBS at 4°C overnight and incubated in 96% ethanol. Fat was removed by incubating in acetone and embryos were stained with 0,015% Alcian Blue (A5268-10G, Sigma-Aldrich) /0,005% Alizarin Red (a5533-25g, Sigma-Aldrich) in 5% acetic acid, 60% ethanol. Surrounding tissue was cleared with 1% potassium hydroxide and skeletons were stored in glycerol.

Histology

Tissues were fixed in 4% PFA/PBS overnight at 4° C, dehydrated, embedded in paraffin and cut into 5μ m thick slices. Sections were stained with hematoxylin (SLCN6532, Sigma-Aldrich) and eosin (SLCP2819, Sigma-Aldrich) by using standard protocols and analyzed with a Zeiss Axio Imager.Z1 microscope.

RNA in situ hybridization

Digoxogenin labeled cRNA probes were generated by *in vitro* transcription of 1μg template DNA with the RNA DIG labeling kit (#11175025910, Roche) according to the manufacturer's protocol. Tissue slides were de-waxed with Shandon Xylene Substitute (#9990505, Thermo ScientificTM), re-hydrated, fixed with 4% PFA/PBS and proteins were removed by incubation with Proteinase K (P2308, Sigma-Aldrich). After acetylation with acetic anhydride (#242845, Sigma-Aldrich) the labeled probe was mixed with hybridization buffer (10mM Tris ph 7,5; 500mM NaCl; 1mM EDTA; 0,25% SDS; 10% Dextran sulphate; 1x Denhardts's (0,02% FicoII 400; 0,02% Polyvinylpyrolidone; 0,02% BSA); 200μg/ml yeast tRNA; 50% formamide), applied to the slide and hybridization was carried out at 65°C. RNA was digested and slides were washed with decreasing salt concentrations. Specific hybridization was visualized by incubating slides with anti-Digoxigenin-Alkaline phosphatase antibody (1:2000) (#11093274910, Roche) and BM purple AP substrate (#11442074001, Roche). The reaction was stopped with NTMT (100mM NaCl; 100mM Tris pH 9,5; 50mM MgCl2; 0,1% Tween–20), slides were covered with glycergel mounting medium (C0563, Dako).

Flow cytometry

For identifying mesenchymal markers of bone marrow derived cells, Wt MSCLC and EF^{Prx1} MSCLCs were harvested with Accutase (A1110501, Gibco). A total of 0.5 × 10⁶ cells were washed with PBS then transferred to FACS tubes and centrifuged for 5min at 400g. Cells were incubated with specific individual monoclonal antibodies, conjugated with phycoerythrin (PE), allophycocyanin (APC) and allophycocyanin/cyanine7 (APC/Cyanine7) in CliniMACS-buffer (130-021-201, Miltenyi Biotec GmbH) for 30 min in the dark at room temperature. The following cell surface antigens were assessed: CD90-2-APC (17-0902-82, eBioscienceTM), CD44-PE (12-0441-82, eBioscienceTM), CD45-APC (17-0454-82, eBioscienceTM) and CD19-APC-Cy7 (115501, Biolegend). Mouse isotype-matched IgG served as a negative control. Flow cytometry was performed on a *BD LSRFortessaTM Cell Analyzer* and data were processed with FCS express software 7. For immunofluorescence staining the following antibodies were used: YAP (D8H1X) XP (#14074, Cell Signaling).



Cell proliferation assay

Cell proliferation differences between parental and hormone activated/reprogrammed cells were assessed using the CellTiter-Glo Luminescent Cell Viability Assay (Promega, G7570) according to the manufacturer's protocol. One day prior to the assay, cells were seeded in triplicate in 96-well plates at a density of 10,000 cells/100 µl per well, with or without IGF-1 depending on the experimental conditions, and incubated at 37°C with 5% CO₂. At 24, 48, and 72 hours post-incubation, an equal volume of CellTiter-Glo reagent (diluted 1:4 in DPBS) was added to each well. Plates were then incubated in the dark, shaking at room temperature for 10 minutes. Luminescent signals were recorded using a TECAN Spark Cyto plate reader.

Differentiation assays

 1×10^5 Wt MSCLC and EF^{Prx1}MSCLCs were seeded into a six-well plate. For adipocyte differentiation, we used MesenCult medium containing 10% adipogenic stimulatory supplements (#5507, Stem Cell Technologies). At day 21, cells were rinsed with PBS twice and fixed with 4% PFA for 60 min. Cells were then rinsed with distilled water and incubated in 60% isopropanol for 2 min. Finally, cells were covered with Oil Red O solution (O0625, Sigma-Aldrich) for 5 min. Osteogenic differentiation was performed by using the MesenCult osteogenic stimulatory kit (#5504, Stem Cell Technologies). Medium was changed every 2 days, and the cells were analyzed after 21 days of differentiation. After fixation with PFA for 60 min, cells were washed with ddH2O and stained with fresh Alizarin Red S solution and incubated at room temperature in the dark for > 45 minutes followed by 4 washing steps with ddH₂O. Chondrogenic differentiation was achieved using the MesenCult-ACF Chondrogenic Differentiation Kit (#5455, StemCell Technology). After fixation with PFA for 60 min, cells were rinsed with PBS and stained with 1% Alcian blue solution prepared in 0.1 N HCL for 30 minutes followed by 3 washing steps with water.

Soft agar assay

For soft agar assays, each well of a twelve-well plate was first covered with an underlayer of 0.6% SeaPlaque GTG agarose (#50111, Lonza,) in growth medium (RPMI1640 supplemented with penicillin/streptomycin and glutamine). Then, cells were seeded at a density of 1×10^3 cells per well in growth medium containing 0.3% agarose. Upon agarose solidification, plates were incubated at 37° C and 5% CO2%. After 4 weeks, plates were imaged, and colonies were counted.

In vivo tumor formation assay

2.5 × 10⁶ cells/ml in PBS were subcutaneously injected into six to eight weeks old immunodeficient SCID mice (C.B-17/IcrHsd-Prkcdscid; Charles River Laboratories). Tumor formation was examined periodically by palpation. The tumor volume was calculated from tumor size by the formula (diameter × diameter × length/2). The animals were sacrificed, and tumors were surgically removed 31 days after injection. All experiments were performed according to the Austrian guidelines for animal care and protection and were approved by the Austrian ministry for science and research under the license number BMBWF-66.009/0233-V/3b/2019. 2-way anova was used to compare tumors formed by hr-EF^{prx1}MSCLCs and EF^{prx1}MSCLCs.

SiRNA knockdown

For silencing of Yap1, cells were transfected with ON-TARGETplus SMARTpool mouse siRNAs against Yap1 (#L-012200-00-0005, Dharmacon/Horizon) using Oligofectamine reagent (#58303, Invitrogen/Thermo Fisher Scientific). As a control, ON-TARGETplus non-targeting pool (D-001810-10-20, Dharmacon/Horizon) was used. After 24h, the transfection procedure was repeated, and cells were collected for qPCR and Western blot.

Viral Cas9 and sgRNA expression vectors

Lenti-X293T cells were transfected with 10 μ g of LentiCRISPR /Yap1 sgRNA Crispr/Cas9 all in-one lentivector set mouse (#50584114, abcam), 5 μ g of psPAX2 (#12260, Addgene), and 5 μ g of pMD2.G (#12259, Addgene) using Lipofectamine 2000 (#11668019, Invitrogen Corporation) according to manufacturer's instructions. After at least 48 hours of incubation, the virus-containing supernatant was harvested and concentrated using Lenti-XTM Concentrator (#631231, Takara) at 4°C overnight. After centrifugation at 1,500 x g for 45 minutes at 4°C, the pellet was resuspended in one hundredth of the original volume using complete RPMI1640 medium. 10^5 target cells were seeded per well in a 24-well plate for 24 hours prior to viral infection with 0.5 ml of virus suspension in complete medium in presence of 8 μ g/ml Polybrene (TR-1003-G, Millipore Sigma).

Drug synergy assay

For estimation of synergy we used an established Bliss drugs' independence model ¹⁰⁶. According to the Bliss model, drugs act independently if the surviving fraction of cells upon simultaneous administration is equal the product of surviving fractions when drugs are given separately ¹⁰⁷. In order to capture complex drug interaction patterns across dose pairs, dose–response matrices were used, as synergy may exist only for specific pairs of treatment doses. Triplicate dose matrices were generated for each drug pair, positioned in different screening plates (ViewPlate-96, White 96-well Microplate with Clear Bottom, #6005181, PerkinElmer) and based on the fold dilutions of the 72h IC₅₀ values (determined beforehand for each drug). Cell viability was determined after combinatorial drug treatment using CellTiter-Glo® Luminescent Cell Viability Assay (#G7570, Promega), and the Bliss-predicted inhibition was calculated





and compared to the observed values to quantify the interaction between the drugs for each matrix position (additive if = 0 and non-additive if \neq 0; within non-additive cases, it is synergistic if > 0, or antagonistic if < 0).

RNA sequencing

Library preparation and sequencing

To prepare samples for RNA sequencing, total RNA was isolated using Trizol or RNeasy Mini Kit (#74106, QIAGEN). The library was prepared from these samples by poly(A) enrichment and sequenced with 50 bp single-end read mode on an Illumina HiSeq instrument at the Biomedical Sequencing Facility (BSF) at the CeMM Research Center for Molecular Medicine of the Austrian Academy of Sciences (data for Figure S3) or the Vienna BioCenter Next Generation Sequencing Core Facility (VBCF-NGS; all other RNA-seq data).

Data processing and analysis

Raw sequencing data were processed using the nf-core/rnaseq v3.14.0 pipeline, ¹⁰⁸ including alignment to the GRCm38.p6 mouse reference genome and gene-level read quantification using the Ensembl v99 gene annotations. Following initial data processing, all subsequent analyses were performed in R v4.2.2 using Bioconductor packages. The read counts were loaded into DESeq2 ³⁹ v1.38.3 or variance-stabilizing transformation and differential analysis (default parameters). Transcripts with an FDR-adjusted P-value <= 0.05 and an absolute log₂ fold change >= 1 were considered significant. All differential expression analysis results are reported in Tables S2, S6, and S7. For functional enrichment analysis we performed hypergeometric tests using the hypeR package v1.14.0 ¹⁰² and the following databases from enrichR ¹⁰⁹: "TF_Perturbations_Followed_by_Expression", "MSigDB_Hallmark_2020", "ChEA_2022", and "KEGG_2021_Human". As a background for this analysis, we used all genes identified in our analysis. Terms with an FDR-adjusted P-value <= 0.05 were considered significant. For gene set enrichment analysis, we used fGSEA ⁴³ v1.24.0 and the DESeq2 test statistic as a ranking criterion. Gene signatures from Kinsey at al ¹¹⁰. and Riggi et al ¹¹¹. were obtained from MSigDB ¹¹². All enrichment results are reported in Tables S3 and S8.

ATAC-seq

Library preparation and sequencing

ATAC-seq was performed following published protocols ⁴². Briefly, 20,000 to 50,000 cells were lysed in a buffer containing digitonin (#16359, New England Biolabs) and Tn5 transposase enzyme (Tagment DNA Enzyme and Buffer Kit, #20034197, Illumina). After incubation at 37°C for 30 minutes, tagmented DNA was purified and enriched. ATAC-seq libraries were prepared for samples of the following experimental conditions: wt MSCLC (n = 5; N.B., one sample failed quality control in the subsequent analysis, see below), wt MSCLC with IGF-1 (n = 1), EF^{Prx1} MSCLC (n = 4), hr-EF^{Prx1} MSCLC (n = 2), transplant-hr-EF^{Prx1} MSCLC (n = 1) for sequencing. Sequencing was done in 50 bp single-end read mode on an Illumina HiSeq instrument at the Biomedical Sequencing Facility (BSF) at the CeMM Research Center of Molecular Medicine of the Austrian Academy of Sciences.

Data processing and analysis

Raw sequencing data were processed using pypiper v0.10.0 and PEPATAC v0.8.6 103 with MACS2 v2.1.0 104 for peak calling. Following initial data processing, all subsequent analyses were performed in R v4.2.2 using Bioconductor packages. Only samples with a Non-Redundant Fraction (NRF) >= 0.5, a PCR bottlenecking coefficients PBC1 >= 0.7 and PBC2 >= 3, and an TSS enrichment score >= 10 were considered for further analysis (one wt MSCLC sample failed these criteria; see https://www.encodeproject.org/ data-standards/terms/ for a definition of these terms). After merging peaks across all ATAC-seq datasets and removing peaks that overlapped blacklisted regions from ENCODE (https://sites.google.com/site/anshulkundaje/projects/blacklists), we counted for each input dataset the number of reads overlapping the retained peaks with featureCounts (Rsubread v2.12.3) 113. The raw read counts were loaded into DESeq2 39 v1.38.3 or variance-stabilizing transformation and differential analysis (using a "batch" as a covariate; other parameters: IfcThreshold=log2(1.5), independentFiltering=TRUE). Peaks with an FDR-adjusted P-value <= 0.05 were considered significant. All ATAC-seq peaks and differential accessibility results are reported in Tables S4 and S5, respectively. For functional enrichment analysis we performed hypergeometric tests using the hypeR package v1.14.0 102 and the following databases from enrichR 109: "GO_Biological_Process_2021", "PanglaoDB_Augmented_2021", "TF_Perturbations_Followed_by_Expression", and "TRRUST_Transcription_Factors_2019". As a background for this analysis, we used all genes associated with at least one peak in our analysis (i.e., genes whose transcription start site was within 100kb of a peak). Terms with an FDR-adjusted P-value <= 0.005, a log2 odds ratio >= log2(2), and with >= 10 genes in the overlap were considered significant. For motif analysis, we used motifmatchr v1.20.0 114 to scan all ATAC-seq peaks for matches to known motifs from the JASPAR2022 114 database (R package v0.99.8). We then used base R functions to calculate Fisher's exact test (one-sided), considering motif hits with an FDRadjusted P-value <= 0.005, a log2 odds ratio >= log2(2), and occurring in >= 5% of peaks as significant. To identify GGAA microsatellite repeats, we used a regular expression. We then used fast gene set enrichment analysis (fgsea 43 v1.24.0) using the DESeq2 test statistic as a ranking criterion to test for enrichments. All enrichment results are reported in Table S9.

Low coverage whole genome sequencing (IcWGS)

Library preparation and sequencing

lcWGS was performed for Wt MSCLC, EF^{Prx1} MSCLC and hr-EF^{Prx1} MSCLC. Genomic DNA was extracted using the Monarch® Genomic DNA Purification Kit (#T3010S) and sequencing service was utilized running on an Illumina NovaSeq 6000 platform. A



minimum of 100 ng of DNA was sent to and sequenced by Eurofins Genomics. This service included preparation of a 450 bp DNA sequencing library using a modified version of the NEBNext UltraTM II FS DNA Library Prep Kit for Illumina and sequencing on an Illumina NovaSeq 6000 with S4 flowcell, XP workflow and in PE150 mode (Illumina).

Data processing and analysis

Raw sequencing data were processed using the nf-core/sarek v3.2.1 ¹¹⁵ pipeline and aligned to the Mus musculus mm10 reference genome. Copy number variations were inferred using the CNVKit toolkit v0.9.9 ¹¹⁶, integrated into the sarek v3.2.1 pipeline ¹¹⁵. Visualization of the results for specific regions of interest was carried out through a custom Python3 script.

QUANTIFICATION AND STATISTICAL ANALYSIS

Soft-agar colony numbers greater than 0.5 mm in diameter were quantified using ImageJ software (version 1.52). The data were analyzed using GraphPad Prism 8 (GraphPad Software, San Diego, CA, USA) with One-Way ANOVA followed by Tukey's post-hoc test for multiple comparisons. RT-qPCR data are presented as mean ± SE. The statistical significance was determined using a one-sided, paired Student's t-test. The number of observations and statistical details of experiments can be found in the figure legends. Volumes of tumors arising in mice transplanted with parental EF^{Prx1} and derived hr-EF^{Prx1} MSCLC in SCID mice were analyzed using GraphPad Prism 8 (GraphPad Software, San Diego, CA, USA) applying Two-Way ANOVA. Bioinformatic analyses of genomics data and associated statistical tests were performed in R (v4.2.2). Tests used for individual analyses, the number of observations, and measures of centrality are defined in the respective figure legends and in the Methods Details.